

General Disclaimer

One or more of the Following Statements may affect this Document

- This document has been reproduced from the best copy furnished by the organizational source. It is being released in the interest of making available as much information as possible.
- This document may contain data, which exceeds the sheet parameters. It was furnished in this condition by the organizational source and is the best copy available.
- This document may contain tone-on-tone or color graphs, charts and/or pictures, which have been reproduced in black and white.
- This document is paginated as submitted by the original source.
- Portions of this document are not fully legible due to the historical nature of some of the material. However, it is the best reproduction available from the original submission.

**TECHNICAL AND INVESTIGATIVE SUPPORT FOR HIGH
DENSITY DIGITAL SATELLITE RECORDING SYSTEMS**

Progress Reports #12 - 15

Covering Reporting Period July - October, 1982

NASA Contract No. NAS5-26493

IITRI Project No. K06003

**(NASA-CR-170598) TECHNICAL AND
INVESTIGATIVE SUPPORT FOR HIGH DENSITY
DIGITAL SATELLITE RECORDING SYSTEMS**

N83-36439

Progress Report, Jul. - Oct. 1982 (IIT

Unclas

Research Inst.) 80 p HC A05/MF A01 CSCL 01B G3/35

44012

Prepared for:

**Mr. C. Powell, Code 728
NASA/Goddard Space Flight Center
Greenbelt Road
Greenbelt, Maryland 20771**

Prepared by:

**R. A. Schultz
Associate Engineer
Magnetic Recording
IIT Research Institute
10 West 35th Street
Chicago, Illinois 60616**



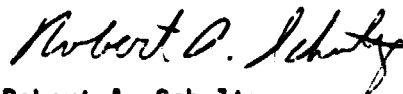
October 1982

FOREWORD

This progress report covers the 12th through 15th monthly periods on IITRI Project K06003 (formerly E06514) entitled "Technical and Investigative Support for High Density Digital Satellite Recording Systems." The work reported herein was conducted for NASA/Goddard Space Flight Center under Contract No. NAS5-26493 during the period July - October, 1982. This report contains results from the surface defect analysis of tape types 3M 5198 and Fuji H621. Conclusions and plans for future investigations are presented in the final section. C. Donald Wright acted as the project leader and Robert A. Schultz conducted the technical investigations with assistance from Theodore Shafer, Frank Jaworski, and Brian Filar. John Brown of Walter C. McCrone Associates performed the SEM and EDAX procedures.

Data for this report are recorded in IITRI Logbooks C26764 and C26765.

Prepared by



Robert A. Schultz
Associate Engineer
Engineering Research Division

APPROVED:



Henry G. Tobin, Manager
Instrumentation & Controls
Engineering Research Division

TABLE OF CONTENTS

<u>Section</u>	<u>Page</u>
1.0 INTRODUCTION.	1
2.0 DROPOUT MODEL	3
3.0 DROPOUT AND DEFECT CHARACTERIZATION	9
3.1 Dropout Size	10
3.2 Dropout Signal Profiles.	11
3.3 Dropout Reproducibility.	13
4.0 PROCEDURES.	14
4.1 3M 5198 Reel History	14
4.2 Fuji H621 Reel History	15
4.3 Dropout Mapping and Defect Identification.	15
4.4 Interference Microscopy.	17
4.5 Scanning Electron Microscopy	18
4.6 Energy Dispersive X-Ray Analysis	18
5.0 RESULTS	20
5.1 Results from 3M 5198	22
5.2 Results from Fuji H621	57
6.0 CONCLUSIONS AND FUTURE DROPOUT MEASUREMENTS	68
6.1 Dropout Dimensions and Distribution.	68
6.2 Surface Defect Analysis.	70
6.3 Measurement of Dropout Performance During Extended Tape Use	72
6.4 Head Selection and Data Analysis	73
6.5 Measurement of Phase Related Bit Errors.	75

LIST OF TABLES

<u>Table</u>	<u>Page</u>
3.1 Electrical Dropout Characteristics.	9
4.1 X-Ray Energies of Elements Detected by EDAX	19
5.1 Dropout Measurements Following the Virgin Recordings and a Second Recording of 3M 5198 and Fuji H621	21
5.2 Head to Tape Separation Resulting from Tenting.	36

LIST OF FIGURES

<u>Figure</u>		<u>Page</u>
2.1	Track/defect geometry of model defects.	4
2.2	Effect of distance between defect center and track center on dropout length.	7
3.1	Dropout signal profiles for calculated model defects.	12
5.1	Oxide and defect surface at 3M 5198 base film asperity.	25
5.2	Surface profile at 3M 5198 base film asperity	26
5.3	EDAX of normal 3M 5198 oxide binder and foreign body.	28
5.4	SEM and EDAX of a small particle.	29
5.5	Surface profile at defect 3M 5198-40-A.	31
5.6	Interference micrograph of defect 3M 5198-41-A.	33
5.7	Tenting effect around defect.	35
5.8	SEM and EDAX of defect 3M 5198-00-C	39
5.9	SEM of oxide surface near defect 3M 5198-01-C	41
5.10	SEM of deposit at defect 3M 5198-05-C	43
5.11	SEM and EDAX at defect 3M 5198-12-C	45
5.12	Dark field micrograph of deposit array at defect 3M 5198-32-C	48
5.13	SEM and EDAX of defect 3M 5198-32-C	49
5.14	SEM and EDAX of defect 3M 5198-34-D	51
5.15	SEM of defect 3M 5198-35-D.	52
5.16	SEM of defect 3M 5198-36-D.	54
5.17	SEM of defect 3M 5198-37-D.	55
5.18	EDAX of normal Fuji H621-01	59
5.19	Bright field and interference micrographs of defect Fuji H621-01.	60
5.20	SEMs of defect Fuji H621-01	62
5.21	EDAX of inclusions at defect Fuji H621-01	63
5.22	SEM and EDAX of defect Fuji H621-02	64
5.23	SEM and EDAX of defect Fuji H621-03	66

TECHNICAL AND INVESTIGATIVE SUPPORT FOR
HIGH DENSITY DIGITAL SATELLITE RECORDING SYSTEMS:
MAGNETIC TAPE SURFACE DEFECT ANALYSIS

1.0 INTRODUCTION

Dropout detection and measurements employ a continuous constant frequency signal and tape speed that produce a wavelength equal to two bit lengths on the tape. This procedure insures that the tape is tested under standardized high resolution conditions, and since record and reproduction losses generally increase with frequency, the continuous dropout test signal at the maximum possible frequency produced by digital coding constitutes a worst case test condition. With high density digital recording (HDDR), the test signal frequency approaches the upper band edge of the recorder system response, where only surface layers of the oxide coating contribute significantly to record and reproduction, and where head to tape spacing losses tend to be greatest. Since dropouts are most often associated with spacing losses, the physical defects that cause dropouts should be surface phenomena. Therefore, a search for the causes of dropouts becomes a surface defect analysis.

The major objective of the surface defect analysis was to locate, measure and characterize oxide coating defects that are large enough to cause 20 dB dropouts on a 7 mil wide track. The study also provided information regarding the improvement in dropout performance following an initial period of use as compared to the dropout performance of virgin tape, and indications of the frequency of occurrence for various types of surface defects. The general technique of the analysis was the location of defects by electronic detection and optical microscopic examination followed by measurement and analysis with optical, SEM and microanalytical techniques. Prior to presenting details of the techniques, a simple dropout model is presented. The model shows how electronic dropout length can be related to defect location relative to the track and an assumed physical structure which may approximate some typical oxide surface defects.

This report discusses dropout and defect classification with emphasis on how surface defects responsible for electronic dropouts were identified, what effect various defects could have on the application of tapes to satellite tape recorders (STR), and what types of defects might be field correctable after production of the tape but prior to installation in the STR.

Any physical separation between the oxide surface and the gaps of the record and/or reproduce heads will cause a reduction in the reproduced signal level. The magnitude of the loss during reproduction is often approximated by the "Wallace" formula:

$$\text{spacing loss} = 54.6 \frac{d}{\lambda} \text{ dB}$$

where d is a uniform head to tape spacing across the track width and λ is the recorded wavelength. If the STR can recover data during a 20 dB signal loss, then a uniform head to tape spacing greater than 22 microinches across the entire track during reproduction of a normally recorded 60 microinch wavelength could result in a failure to recover the data represented by the signal. Record spacing loss also increases with the head to tape spacing and with decreasing wavelength, but this loss is probably a more complex function of wavelength than the Wallace formula and has not been measured for the subject tape types. The important consequence of spacing losses during both record and reproduce processes is that in order to produce a given loss of signal, the dimensions of a defect fixed at one location on the oxide surface during both record and reproduction need not be as great as the dimensions of a loose particle that changes locations between recording and reproduction. In addition, electrical dimensions of a dropout caused by a fixed defect can be reduced if the physical dimensions of the defect can be reduced by cleaning or normal use of the tape. This effect is very pronounced in the results reported below. These considerations place a high degree of importance on the nature and abundance of various defect types, the generation of new defects during the life of a tape, and the possibility of head clogging due to deposition of defect materials onto the head during the life of the STR.

2.0 DROPOUT MODEL

The dropout model assumes that a surface defect results in a circular area over which no change of magnetic flux is sensed by the reproduce head, and that normal flux changes are sensed outside of this area. Since the reproduced signal level is directly proportional to the rate of change in magnetic flux sensed by the head, an immediate consequence of this assumption is that the circle must overlap at least 90% of the track width in order to produce a dropout defined by a 20 dB signal reduction. Thus the minimum effective diameter of a surface defect located near the center of a 7 mil track is greater than 6 mils, and greater effective widths are required for dropouts when defects are not centered over the track.

The circular effective area will be approached by a physical defect such as a fixed 0.1 mil projection from the oxide surface if the tenting action around the projection causes an increase in the head to tape spacing much greater than the 10 microinch order of magnitude suggested by the Wallace formula over a distance much less than the effective diameter of the defect. This intuitive approach eliminates integration of spacing losses as complicated functions of defect shapes and tenting across the track width. The dropout model relates lengths of dropouts to the defect/track geometry and detection threshold. It enhances intuitive insight of mechanisms responsible for dropout depth profiles, repeatability, and detection efficiency for various track widths and spacing. However, the flux density changes caused by real defects must be much more complex and variable than the model assumption, and the model cannot be used to calculate defect sizes or shapes from electrical measurements with any degree of precision.

Figure 2.1 illustrates the two general cases of the model defect/track geometry. A 12 dB signal reduction is employed to define the dropout for illustrative clarity, but the model can be extended to any threshold level. The 12 dB level and the circular area assumption imply that the dropout occurs when at least three-fourths of the track width is covered by the defect width. In case I the dropout length L is determined by inscribing a rectangle of width $3W/4$ within the circular defect area where W is the track width. For a general threshold level, the width of this rectangle

ORIGINAL PAGE IS
OF POOR QUALITY

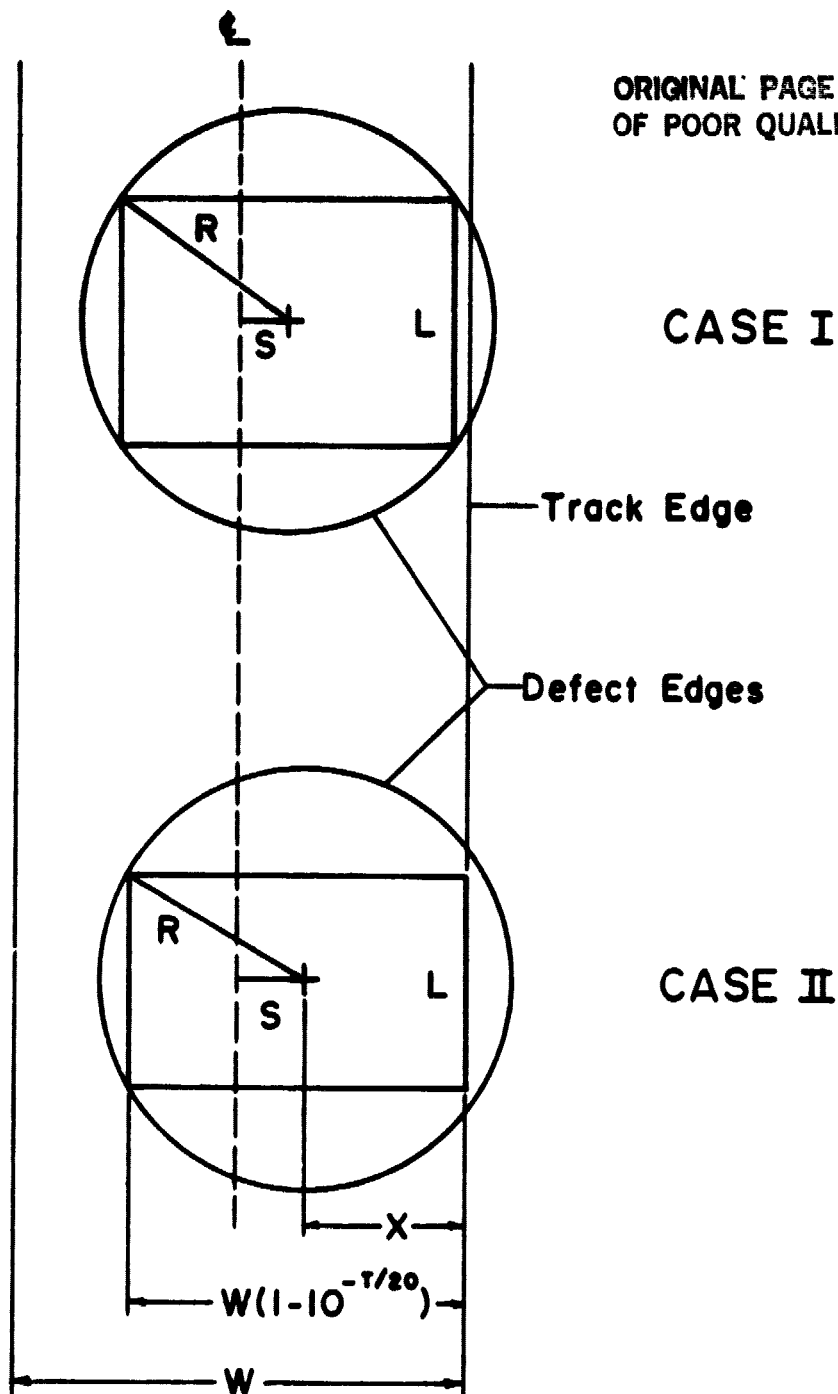


Figure 2.1: Track/defect geometry illustrating dropout length for a dropout threshold $T=12$ dB. In case I, a rectangle of width $3W/4$ inscribed within the circular model defect area determines the dropout length for track center to defect center distance $S < \frac{1}{2}W (10^{-T/20})$. In case II where $S > \frac{1}{2}W (10^{-T/20})$, the width requirement imposed by the threshold places one edge of the dropout rectangle along the track edge, reducing its length. Analytical relationships are specified in the text.

becomes:

$$W (1-10^{-T/20})$$

where T is the defining dropout threshold in decibels. The length and width of the inscribed rectangle are related to the defect diameter by the Pythagorean theorem:

$$(2R)^2 = L^2 + (W (1-10^{-T/20}))^2$$

so the length in case I is:

$$L = 2 \sqrt{R^2 - (\frac{1}{2} W (1-10^{-T/20}))^2} \quad (\text{Case I})$$

In case II, the track center to defect center distance S has been increased so that the rectangle inscribed for case I would no longer fall within the limits of the track edges, but a rectangle of width $W (1-10^{-T/20})$ can still be inscribed between the track edge and the defect edge. Now the Pythagorean relationship becomes:

$$R^2 = (\frac{L}{2})^2 + (W (1-10^{-T/20}) - x)^2$$

where $x + S = \frac{W}{2}$ or $x = \frac{W}{2} - S$. Substituting and solving for the length yields:

$$L = 2 \sqrt{(R^2 - S + W (\frac{1}{2} - 10^{-T/20}))^2} \quad (\text{Case II})$$

The two cases are equivalent when $S = \frac{1}{2} W (1-10^{-T/20})$. Case I occurs when $S < \frac{1}{2} W (1-10^{-T/20})$ and case II occurs when $S > \frac{1}{2} W (1-10^{-T/20})$. In the current report $W = 7$ mils and $T = 20$ dB so the transition from case I to case II occurs at a track center to defect center distance greater than 0.35 mils. For large diameter defects, case I can be neglected when the threshold is high (>20 dB). As S increases, the dropout length decreases, slowly at first but with increasing rate until the length becomes zero for $S \geq R - W (\frac{1}{2} - 10^{-T/20}) = R - 2.8$ mils for $W = 7$ mils and $T = 20$ dB.

Figure 2.2 plots this relationship for several defect diameters. The steep slopes of the right sides of the curves as S approaches $R - W (1 - 10^{-T/20})$ indicate that guidance changes have a large effect on dropout length or repeatability as S approaches $R - 2.8$ mils.

The dropout model suggests causes of different dropout rates measured with different track widths. Most of the defects encountered in this study have small effective widths, and the relative abundance of defects must increase for decreasing physical sizes down to the point where defect sizes are too small to effect 20 dB dropouts. At the same time, uniform random distribution of defect center to track center locations has been assumed for large sample areas. With 18 mil tracks, 3 mil guard bands, and 20 dB thresholds employed for initial dropout measurements, 50% of the defect centers are at least 5.3 mils from the nearest track center, and defects with effective radii less than 7.2 mils plus the defect center to track center distance are not counted as dropouts, so that half of the 25 mil wide defects are not counted. Defects with smaller effective widths are detected with decreasing probability, and defects narrower than 16.2 mils cannot effect a 20 dB dropout on an 18 mil track.

With the same 20 dB threshold but 7 mil tracks and 1 mil guard bands, 50% of the defects are within 2.0 mils of the nearest track center, half of the 9.6 mil effective width defects are positioned to cause 20 dB dropouts, and 6.3 mil wide defects that are centered on the track will cause short 20 dB dropouts.

Equivalent thresholds that measure equal lengths for case I model dropouts can be specified by equating two case I length equations for the same defect radius, two known track widths and one known threshold and solving for the unknown threshold:

$$T_2 = -20 \log \left(\frac{W_2 - W_1 (1 - 10^{-T_1/20})}{W_2} \right)$$

which shows that a 3.74 dB threshold and an 18 mil head will measure the same lengths for case I dropouts as a 20 dB threshold and a 7 mil head.

ORIGINAL PAGE 19
OF POOR QUALITY

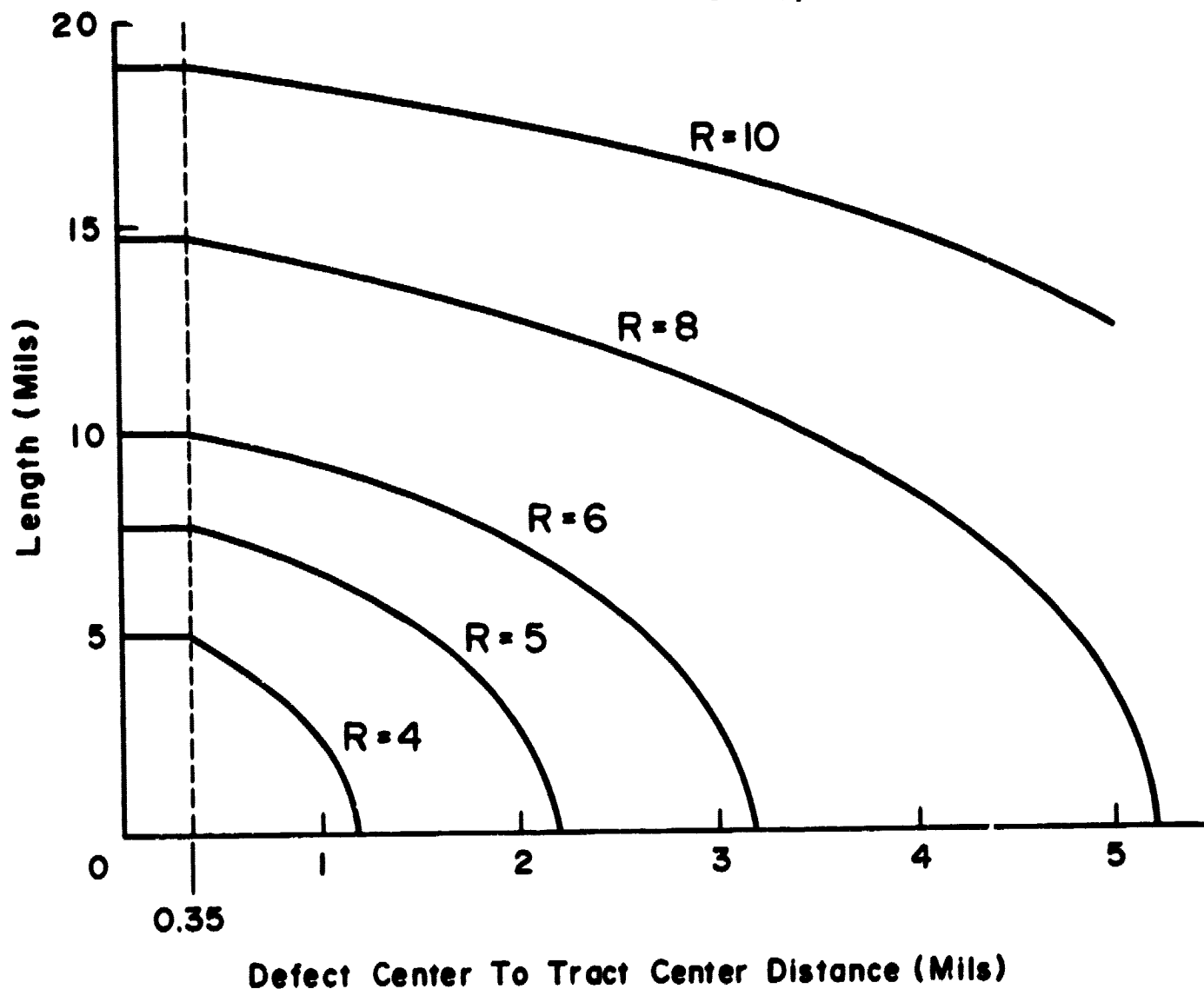


Figure 2.2: Effect of distance between defect center and track center on dropout length calculated for a 7 mil track width and a 20 dB threshold. R is the effective radius of the model dropout. Length is independent of spacing distances less than 0.35 mils. The right edge of each curve is tangent to the vertical.

For defects that cause case I dropouts on one track format and case II dropouts on another format, or case II dropouts on both formats, the equivalent threshold expressions become more complicated functions that include one or both defect center to track center distances as variables. Assuming model behavior, inference of these distances is conceivable with dropout imaging, and deviations of real defects from the model behavior are least significant for the wide multitrack defects that might exceed error correction capabilities of sophisticated HDDR codes. Implications of these effects on threshold selection and criteria for counting dropouts with parameters significant to error detection and correction codes are discussed after presenting results of the defect analysis.

3.0 DROPOUT AND DEFECT CHARACTERIZATION

The electronic dropout detection and measurement techniques employed in this study can locate an oxide surface defect to within a few mils transversely across a tape and a few inches along the tape. Several optically observable surface features may be present within the area defined by electronic measurements. In order to determine which, if any, of the observed surface features causes an electrical dropout, the observed dropout characteristics must be correlated with readily observable physical characteristics of the causative surface defect. Characteristics of dropout size, signal profile and reproducibility are outlined below and are defined or described in the following sections. A few examples of defect types are mentioned to clarify some of the dropout characteristic descriptions, but the examples are not intended as a comprehensive list of defect types or as representative of the common defect types encountered on the subject samples:

TABLE 3.1

Electrical Dropout Characteristics

I. Size

- A. Depth
- B. Length
- C. Width

II. Signal Profile

- A. Shape
- B. Reduced depth near center
- C. Irregular
- D. Closely spaced dropouts

III. Reproducibility

- A. Permanent dropouts
- B. Temporary dropouts

3.1 Dropout Size

Dropouts have three dimensions; length, width and depth. Dropouts are defined as signal reductions below a specified depth over a specified minimum tape length or time. The 20 dB by two bit length (60 microinch) dropout definition employed in this study is close to the measurement limits imposed by the signal-to-noise ratio and finite bit length which prevent the use of maximum depth as a useful parameter. Depth or signal profile as a function of head gap to defect location and changes in depth with defect wear and tracking repeatability are useful and are discussed below. Dropout length is measured in wavelengths where one wavelength equals two bit lengths or 60 microinches for the present study. Length units may be converted to mils (10^{-3} inches) for correlations with physical defects.

The dropout model shows that dropout lengths can vary as a function of track center to defect center distance, and that a single dropout measurement can only place a minimum restriction on the effective width of a defect without locating its center. When a model dropout is measured on several tracks, a maximum effective width is indicated and a maximum measured dropout length approaching the maximum effective defect length usually occurs near the track closest to the defect center. If mirror image symmetry is assumed about the transverse axis of the tape, multi-track dropout measurements produce an image of the effective defect area. The resolution of the image can be increased with multiple measurements on overlapping tracks; a technique that is facilitated by recording a single track across the entire tape width. Defect imaging by multiple dropout measurements may correlate well with surface depression, pits, or smooth surfaced nonmagnetic inclusions where the head to tape spacing coincides with the physical area of the defect. For surface impressions and particles, tenting extends the effective area of the defect beyond its optically observable physical size so that dropout images do not correlate well with defect sizes. The imaging procedure does indicate the center location of the defect and provides a series of signal profiles which may correlate with physical characteristics of the causative defect.

3.2 Dropout Signal Profiles

Dropout signal profiles or depth profiles are the reproduced signal amplitudes as a function of the gap location relative to the defect. They can be observed with an oscilloscope at the filtered output of a diode dropout detector. Depth profiles can be difficult to interpret when the track center to defect center distance is unknown, but multiple track length measurements enable alignment of the track with the defect prior to profile observations. Figure 3.1 plots dropout signal profiles calculated from three model defects to illustrate likely mechanisms for three commonly observed profiles. Curve A results from a circular defect with an effective radius which is too small to cause a 20 dB signal reduction. The larger defect radius employed to calculate Curve B results in a defect that completely covers the track along most of its length, producing an essentially rectangular profile with total elimination of the signal. Both profiles could result from a circular depression or a surface projection of nonmagnetic material such as a base film asperity or a dust particle. The model defect employed to calculate Curve C is a 3 mil radius cylindrical projection of magnetic material on the oxide surface which might result from a calendering defect or a loose oxide binder particle. An effective radius of head to tape separation equal to 5 mils is assumed around the particle as in Curve B, but partial head to tape contact is resumed as the magnetic defect passes across the head gap, resulting in a bilobed signal profile with two amplitude minima.

Irregular signal profiles result when physical defects vary widely from the circular model. Rough surfaces and closely spaced groups of defects can cause irregular profiles. Groups of closely spaced profiles can be associated with groups of closely spaced defects aligned with the track.

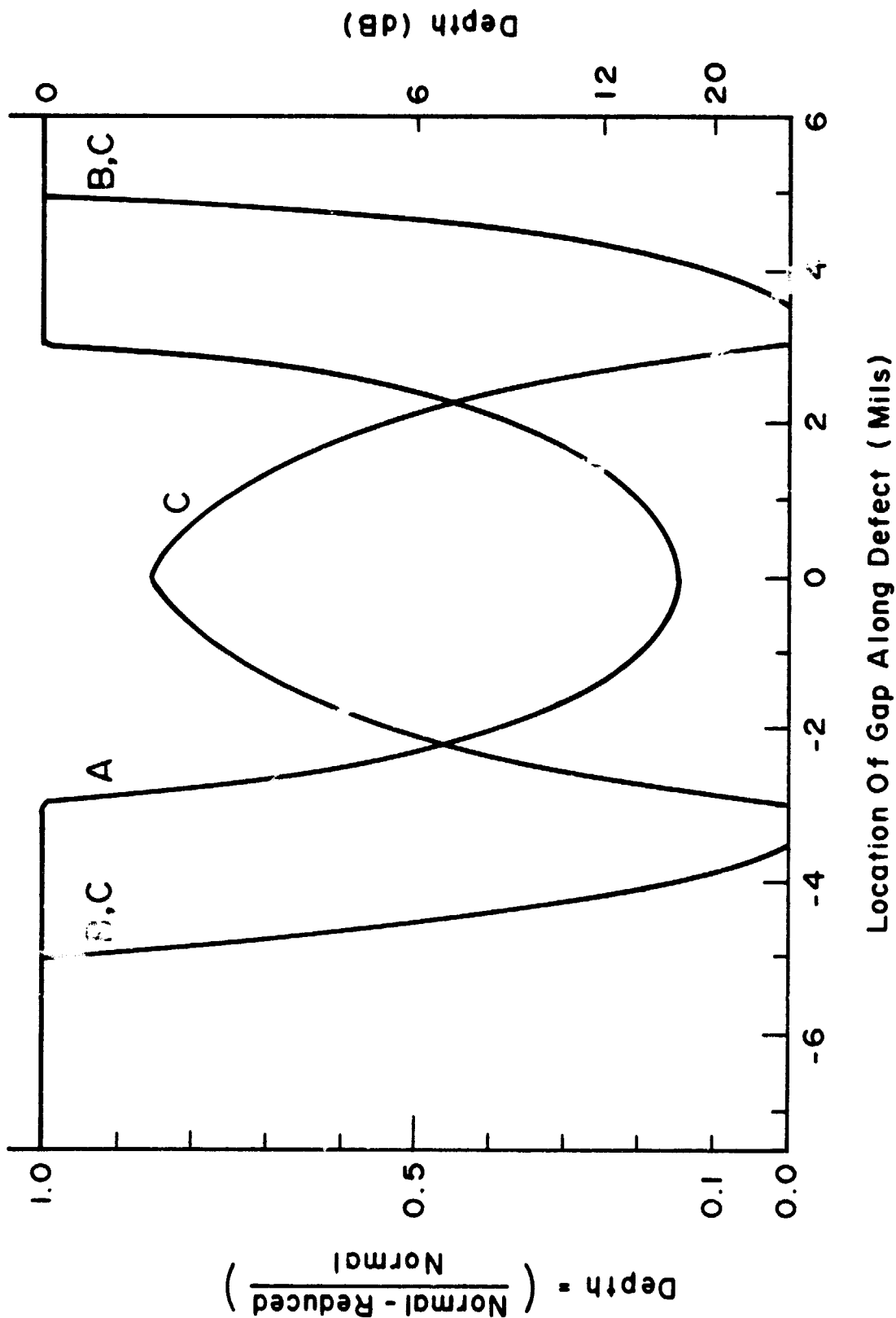


Figure 3.1: Dropout signal profiles calculated for model defects centered over a 7 mil track. Curve A results from a 3 mil defect radius and constitutes a subthreshold profile, Curve B results from a 5 mil defect radius. Curve C assumes a 3 mil radius oxide surface projection with a 5 mil effective defect radius resulting from tenting around the projection. Real defects cause profiles similar to all three of the curves.

3.3 Dropout Reproducibility

All of the shape and size characteristics of dropouts described up to this point are subject to changes from several causes. The temporal nature of dropouts and their causative defects may be of extreme importance in the lifetime reliability of STR tapes, and dropout repeatability will be emphasized in this report both as an aid to identifying the most significant defects and as a parameter for comparing tape types. As anticipated in the introduction to this report, dropout reproducibility is more sensitive to the combination of re-recording and subsequent reproduction than to the action of multiple passes during reproduction alone. The term "permanent" dropout will be used to describe signal losses exceeding the 20 dB dropout defining threshold both before and after a second recording of the subject tape samples, but the definition of permanent dropout should be restricted to dropouts that repeat only after a specified conditioning, cleaning and re-recording procedure or a series of these procedure cycles. The term "temporary" dropout in this report denotes 20 dB losses of signal before or after a second recording but not both.

Loose particles that are moved by tape transport mechanisms between recordings are an obvious potential source of temporary dropouts. Changes of physical defect dimensions due to wear or material deposition is an important mechanism for the class of defects that project from the oxide surface. The dropout model indicates that slight guidance and tracking changes can effect dropout detection when the relative location between the track and the defect approaches a critical value. The probability of this effect increases with decreasing defect width.

4.0 PROCEDURES

Surface defect analysis data were obtained for a single reel of 3M 5198 and a single reel of Fuji H621. This section reviews the history of the reels and presents general procedures that were held constant throughout most of the study. Variations in procedures developed to maintain analytical efficiency while meeting the challenges imposed by the different defect types and densities are discussed in Section 5 along with results obtained from them. In general, the procedures were considered unbiased up to the point of selecting dropouts for defect identification. The permanent dropout distinction may bias the defect identification step toward more significant defect types in addition to improving identification efficiency and reducing erroneous identification. The last 3M 5198 sampling procedure was improved by elimination of possible bias due to previous avoidance of selecting dropouts closely spaced along the tape length.

4.1 3M 5198 Reel History

The 3M 5198 dropouts and defects described in this report were isolated from reel 43056 17 010 24 that had been employed for two earlier dropout measurements presented in progress reports 8-11 for this project. The initial 1600 feet of this 9200 feet by 1 inch reel was recorded at 500 kHz and 30 ips for measurements with 18 mil reproduce tracks, and then the reel was degaussed and recorded at 1.0 MHz and 60 ips for dropout screening with 7 mil tracks. This step constituted the virgin recording for the samples employed in the current study.

The initial 1600 foot segment of this reel was employed for technique development. The remaining tape was screened for dropouts, and that procedure included the virgin record pass followed by thirteen reproduce passes, all over the record head, the 7 mil reproduce head, and two stainless steel dummy heads. An exceptionally high dropout rate was measured on one center track during screening, and center tracks were not sampled during the defect analysis except to identify and analyze the defect responsible for the high dropout rate.

4.2 Fuji H621 Reel History

The Fuji H621 dropouts and defects described in this report were isolated from a lot number 079552 reel employed for dropout screening, described in progress reports 8-11 of this project, and the virgin recording referred to in the present report is the same recording employed in the previous report. Therefore, the virgin recording and preconditioning of this reel prior to the current study is virtually identical with the 3M 5198 reel.

The subject reel exhibited the worst overall dropout performance of the five screened Fuji H621 reels. This high dropout rate was considered helpful for finding a population of varied defects, and reels with better performance were saved for distribution to OEM's.

4.3 Dropout Mapping and Defect Identification

Dropout maps were prepared before and after the second recording of 3M 5198 and Fuji H621 samples. Instrumentation and record parameters were identical to the 7 mil track dropout screening tests described in progress reports 8-11. Reproduce track center-to-center distance was reduced to 5.2 mils in order to increase the detection efficiency for small closely spaced defects and to improve dropout width measurement resolution. The overlapping track spacing is slightly greater than the total uncertainty factor between the head position and the center of the field of view at the optical defect identification station. Maps are analyzed by marking changes in total error registrations on each track, circling changes on adjacent tracks in the same five foot tape segment, and counting each circle as one dropout. An error registration change on any of the same tracks of a given five foot segment of maps prepared before and after the second recording is counted as a permanent dropout without regard to differences in the number of errors or adjacent tracks.

After localizing the permanent defects within five foot tape segments and one or more tracks, the head was repositioned over the track closest to the defect center. With the 60 ips tape speed required for sufficient S/N ratio to detect 20 dB dropouts, the transport cannot be stopped with adequate precision to further localize the defects due to

varying reel inertias. Therefore, dropout signal profiles and tape footage were observed at the point of detection, the tape speed was reduced to 15 ips, and the transport was stopped immediately after observing the time scaled signal profile at the slower speed. Then a numbered adhesive marker was placed on the back side of the tape near the reproduce head across from the sample area. Thus the marker would be about eight inches away from the defect on the supply side, and the distance between the defect and the reference edge of the tape was known from the head position.

Extensive use of the transport shuttle feature during dropout localization insured adequate time for transport speed and AGC stabilization without diverting attention from dropout length measurements or signal profile observations. For most of the tape samples any other permanent dropouts that fell within the shuttle points of a given dropout subjected to the preceding localization procedure were rejected as candidates for further localization and defect identification procedures in order to limit the number of passes over a given defect. All permanent dropouts on 3M 5198 sample D were subjected to the localization and defect identification, but shuttle points were selected with care to insure that the transport did not stop near one permanent dropout while another dropout was being localized.

After the permanent dropout locations on a given tape sample were marked, the sample was cut from the remainder of the reel and was transferred to the defect identification station consisting of motorized hubs to maintain tape tension, flanged rollers that contact the back side of the tape, and an optical microscope that can be positioned precisely across the width of the tape. Several inches of tape were scanned on either side of the points eight inches away from the dropout markers along the take up side of the marker, but the identified defect usually occurred within one inch of the indicated location. In cases where defect identification was uncertain, due to multiple features close to the track center that did not correlate with dropout observations, the dropouts were still classified as permanent features, but the potential defect were not subjected to analysis. Positively identified defects were marked, and detailed optical microscopy, interference microscopy, scanning electron microscopy (SEM) or other microanalytical procedures were selected for each defect with the intent of gaining meaningful information about a wide range of defects.

4.4 Interference Microscopy

Surface profiles of many defects were examined by interference microscopy. These images appear as alternating light and dark bands which should be thought of as the intersection of the tape surface with a set of evenly spaced parallel planes oriented obliquely to the plane of the surface. The intersection of these planes with a perfectly smooth flat surface would produce equal spacing between bands and sharp straight transitions from light to dark bands. Any deviation from a flat surface deflects the bands in proportion to the change in the surface profile and the distance between the parallel planes or the band interval. One band interval constitutes a set of one light band adjacent to one dark band and is equal to 10.6 microinches for thallium illumination or about 12 microinches for white light illumination which can be readily distinguished by uneven band intensities. Band deflections can be measured to one-tenth of an interval providing a resolution of 1 microinch, and the distinguishable band intensities of white light illumination enable a measurement range greater than 150 microinches at sharp profile transitions under optimal conditions. The distance between bands on the surface can be changed by altering the angle of intersection between the bands and the surface.

Although interference micrographs of defects provide accurate measurements of their physical profiles, they do not indicate the effective defect area resulting from the tenting action of a surface projection. The longitudinal tension in the tape, the anisotropic molecular orientation of the base film, and the curved surface of the head may all cause the shape of the tent around a surface projection to deviate from the circular shape of the model. To study these effects, a projecting defect was positioned against a 0.24 inch diameter glass tube to simulate head to defect contact. The back coating at the defect had been removed gently to provide an adequate reflective surface, and the interference micrographs were made of the back surface of the base film at the defect. Assuming that the back surface follows the contours of the oxide surface, the effective width of a constant head to tape separation can be measured as a function of the distance along the tape from the defect for comparison to the circular dropout model. Analysis of these images was simplified by adjusting the microscope so that the parallel planes forming the interference bands are parallel to the axis

of the glass tube. The tape surface that follows the contour of the tubing has straight bands that become narrower as the equidistant parallel planes cut deeper into the cylinder. Head to tape separation at the gap location is measured by counting band crossings along the vertex of the glass tubing, which is at the center of the widest band. The defect location along the tape should coincide with the point of maximum head to tape separation, which is indicated by the line parallel to the tubing that crosses the maximum number of bands.

During interference microscopy, all samples were secured at one end to the microscope stage, and an 8 ounce weight was suspended from the free end of the sample hanging over the edge of the stage. After placing tension on the samples subjected to direct viewing of defects, a glass plate was placed on the back side of the sample to help maintain flatness. The glass tubing was secured to an notched stage insert that produced a 5.3° total wrap angle. Dummy heads and stage inserts can be fabricated to match a specified head contour and wrap angle, which is recommended before attempting additional measurements.

4.5 Scanning Electron Microscopy

All scanning electron microscopy (SEM) specimens were shadowed with gold and were viewed at an angle of 60° with the plane of the tape. The direction of tape travel is horizontal across the SEM image unless otherwise indicated.

4.6 Energy Dispersive X-Ray Analysis

Energy dispersive X-ray analysis (EDAX) produces spectra of X-ray energies emitted by the sample in response to the impinging beam of the electron microscope. Each element is characterized by a set of X-ray emission energies, each with a different intensity. The electron beam can sample a single spot or a raster shaped rectangle placed over the area of interest. Some of the electrons may pass through thin defects, so the spectra can be influenced by elements in the underlying oxide binder. The degree of this influence depends on the defect thickness and material. X-ray energies below 1.0 keV do not penetrate through the beryllium window of the detector, and elements with atomic numbers below sodium (11) are not detectable.

All EDAX spectra in this report have linear scales of 0-10 keV along the horizontal axis. Data collection stops automatically when one peak reaches the maximum counting range, and a cursor allows precise measurements of the spectral energies. Table 4.1 lists elements associated with all of the energy peaks detected during this study. Spectral energies are measured with a calibrated cursor, and slight shifts present on spectra photographs result from parallax errors. Gold results from SEM sample preparation, and some aluminum background usually results from secondary emissions in the microscope. Cobalt peaks at 6.92 keV and 7.65 keV are masked by iron peaks.

Table 4.1
X-Ray Energies of Elements Detected by EDAX

<u>Element</u>	<u>E N E R G Y</u>	
	<u>Primary Peak</u>	<u>Secondary Peak</u>
Sodium	1.04	--
Aluminum	1.49	--
Silicon	1.74	--
Gold	2.12	9.71
Chlorine	2.62	--
Potassium	3.31	--
Tin	3.43	--
Calcium	3.69	--
Chromium	5.41	--
Iron	6.40	7.06
Nickel	7.47	--

5.0 RESULTS

The unbiased dropout counts and length measurements from the tape samples for this report are listed in Table 5.1. Total lengths of dropouts include the lengths of multitrack dropouts registered on each of the overlapping tracks. Permanent dropout counts are determined by comparing dropout maps before and after the second recording of the samples, while total lengths of all permanent dropouts were measured separately on each of the maps. Sample areas are the product of the sample length and the sample width calculated by multiplying the number of tracks by the 5.2 mil track-to-track center spacing and adding $\frac{1}{2}$ track width. The average per square foot for each dropout parameter has been calculated for comparison of the two tape types included in this study. The table also indicates the number of defects subject to analysis from each sample. The table shows that the mapping procedure was not productive for locating permanent dropouts on Fuji H621. The total lengths of dropouts indicated in Table 5.1 include the lengths of multitrack dropouts registered on each of the overlapping tracks. Therefore, the length parameter is actually more indicative of total dropout area and is further weighted toward larger values for wider dropouts.

The small change in total dropout length before and after the second recording of Fuji sample A stemmed largely from a single temporary multitrack dropout on each map. Another wide temporary dropout occurred only on the virgin recording of Fuji sample B. Multitrack dropouts are also indicated on 3M 5198 maps. Widths of multitrack dropouts on 3M 5198 decrease between the first and second recordings at a high rate as reflected by the 75% reduction in the total length of all dropouts compared with the 50% reduction in the dropout counts before and after the second recording of 3M 5198 samples. One significant departure from this trend is documented in the case history of defect 3M 5198-12-C.

Table 5.1
Dropout Measurements Following the Virgin Recording
and a Second Recording of 3M 5198 and Fujit H621

Sample	S A M P L E S I Z E			D R O P O U T C O U N T S				T O T A L L E N G T H O F D R O P O U T S (mils)			
	Length (feet)	Tracks	Area, (inch ²)	Virgin Recording	Second Recording	Permanent	Identified & Analyzed	A L L D R O P O U T S		P E R M A N E N T D R O P O U T S	
								Virgin Recording	Second Recording	Virgin Recording	Second Recording
3M 5198 - A	200	8	95	11	7	5	2	250	42	77	24
3M 5198 - B	250	8	119	17	10	7	2	214	90	36	34
3M 5198 - C	300	20	387	54	28	20	10	663	135	352	94
3M 5198 - D	300	11	219	25	11	5	5	250	88	94	62
3M 5198 Averages per Square Foot	-	-	-	19	10	6	-	242	62	101	38
Fujit H621 - A	300	20	387	8	7	1	0	257	163	4	7
Fujit H621 - B	300	14	275	3	5	0	0	93	22	0	0
Fujit H621 Averages Per Square Foot	-	-	-	2	3	<1	-	76	40	1	2

5.1 3M 5198 Results

Several common features observable on the surface of 3M 5198 were not associated with 20 dB dropouts. Some of them may be responsible for numerous subthreshold signal perturbations noted while observing dropout profiles with an oscilloscope. The following paragraphs describe these common and apparently innocuous features, and the severe repeating defect that was detected during dropout screening. Case histories of individual permanent dropouts are then presented which include dropout length measurements, width indications, and signal profile observations, and the analysis of defects associated with the dropouts. One case history includes the results of the single successful tenting effect measurement. Case history numbers begin with the tape type followed by an arbitrary two digit identification number followed by a letter which indicates the sample from which they were drawn. Samples are lettered in the order in which they are mapped. Experience and technique improvements are believed to have improved defect identification efficiency after obtaining samples A and B, but small projecting inclusions like those described at the end of this section are invisible or easily overlooked during optical identification of defects.

Groups of small features were observed at densities as high as 130 groups/inch² on the surface of 3M 5198. A typical group covers an area 1 to 3 mils wide and 10 to 20 mils long, and consists of ten to twenty individual objects. All objects of one group tend to have the same orientation and shape which may appear circular or oval, but is usually cuneiform. Dimensions of individual features are less than 1 mil and have been observed with profiles greater than 20 microinches. Quite often, several members of a group are closely spaced along the direction of tape travel, followed by other members over a shorter length with different positions across the tape width. Although the circular shapes suggest bubbles, SEM observations indicate that these features are gouges in the tape surface. They may result from a production burnishing process. Three of these features from one group are visible on the right side of Figure 5.15.

Isolated small highly reflective objects are present at a density of 2000/inch². Typically they are less than or equal to 1 mil in diameter and have profiles lower than 5 microinches. They may be undispersed oxide particle agglomerates. Particle orientation in and around agglomerates and gouges, and the possibility of data errors induced by the effects of these features on the phase of reproduced short wavelength signals has not been evaluated. The high densities of gouges and agglomerates, equivalent to rates of 50/second and 800/second respectively with a 7 mil track at 60 ips, suggest that phase induced errors do not occur every time one of these features passes across the head. However, it is possible that under statistically rare circumstances a set of these features aligned across the tape width could cause multitrack phase errors that exceed the error correction capabilities of an HDDR code. Future phase error testing is described in Section 6.5.

Repetitive calendering marks are less common but are typically much longer and wider than agglomerates and gouge groups on the surface of 3M 5198. Circles, arcs and check mark shapes have been observed with typical maximum dimensions of 20 mils in the plane of the tape surface and projecting profiles of 5 microinches. Since these defects are molded by impressions or depressions on process rollers applied to the uncured oxide binder coating, they repeat at regular intervals. Two different intervals of 43 inches and 37 inches have been observed. Their frequency of occurrence suggests that the slight head to tape separation as the gap approaches one of these defects is the probable cause of numerous triangular signal profiles less than 6 dB below the normal reproduce level observed with 3M 5198. Projecting calendering marks may promote redeposits of material from a head or points of increased tape or head wear.

The repeating defect near the center of the subject 3M 5198 reel was of interest as the cause of an error rate (lost wavelengths/10⁶ wavelengths) six times greater than the average for this reel which renders it unsuitable for use with error correction coding techniques that are affected adversely by high dropout rates. On a given track the repeating defect produced series of several closely spaced dropouts with intervening lengths of dropout free tape. A map of 200 feet of tape with eight tracks centered 2.6 mils apart was prepared which showed that the defect affected up to five adjacent tracks, suggesting an effective width of 17 mils. The defect

location across the tape followed a random path along the tape with a maximum variation of 20 mils. The direction of the change in defect location across the tape width reversed seven times over the 200 foot sample. Table 4.5.1 of progress reports 8-11 (page 128) indicates that the average location of the defect was close to the track centered at 502 mils, but atypically high error rates on tracks at 523 and 544 mils suggest that the defect location may wander even farther at some points along the tape. Signal profiles of individual dropouts along a given track spanned the range of possibilities shown in Figure 3.1, but bi-lobed profiles somewhat less pronounced than curve C seemed to pre-dominante.

Samples of the repeating defect responsible for this high dropout and error rate have been isolated from several points along the reel length. One defect occurs every 17 inches along the tape. Figure 5.1 is a photomicrograph of the oxide surface at one of the defects showing a 3.8 mil by 4.8 mil ovoid shape with scribed lines in the direction of tape travel suggesting surface wear. When the back coating was removed for the tenting profile procedure, a similar size structure was observed on the side of the base film opposite the oxide coating, indicating that the repeating defect extends through the base film. This was verified by removing the oxide coating at the defect and noting that the original worn surface of the base film asperity remained intact. Figure 5.2 shows that a randomly selected copy of the defect projects 42 microinches above the oxide surface and 85 microinches above the base film surface immediately adjacent to the worn surface. Note that the difference between the projection heights does not equal the normal oxide coating thickness. The dropout length caused by this defect has not been determined due to the 5 foot sample lengths currently employed which contain multiple copies of the defect.

Since this defect constitutes a surface projection that includes an absence of oxide, the bi-lobe signal profiles cannot be explained by the model dropout employed to calculate Curve C of Figure 3.1. However, the profiles around the exposed base film asperity show that the oxide coating around it gradually increases in thickness to make a smooth transition with the worn asperity surface. Since the worn surface is slightly

Original
OF POOR QUALITY

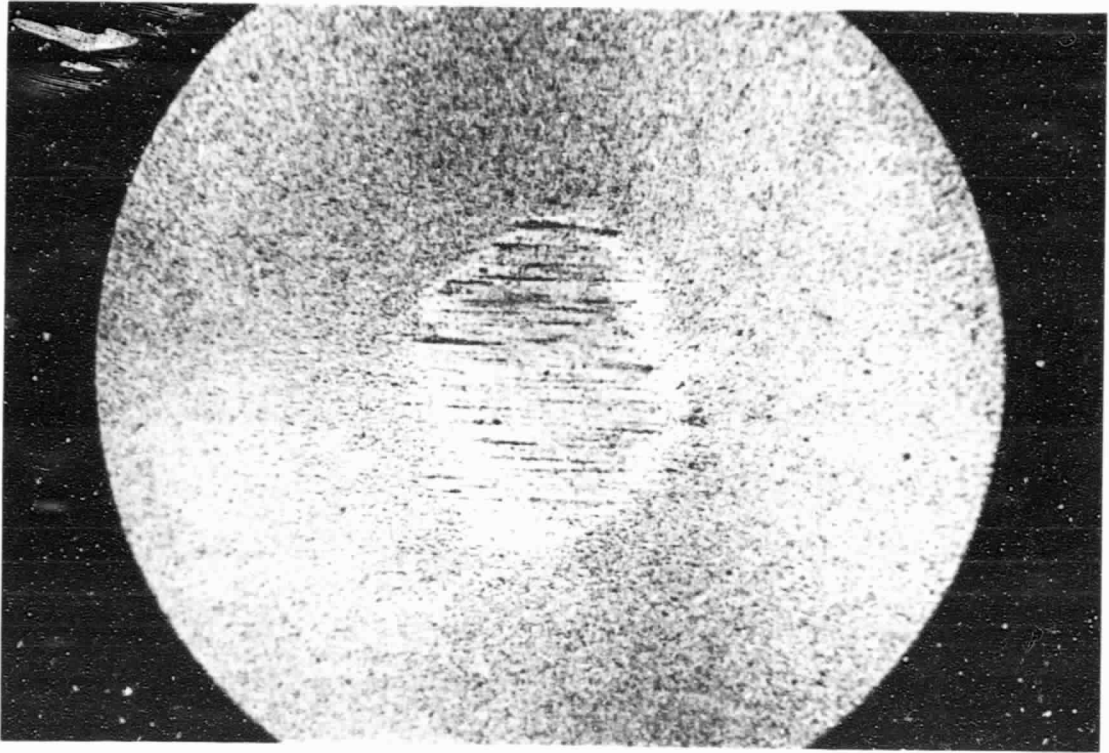
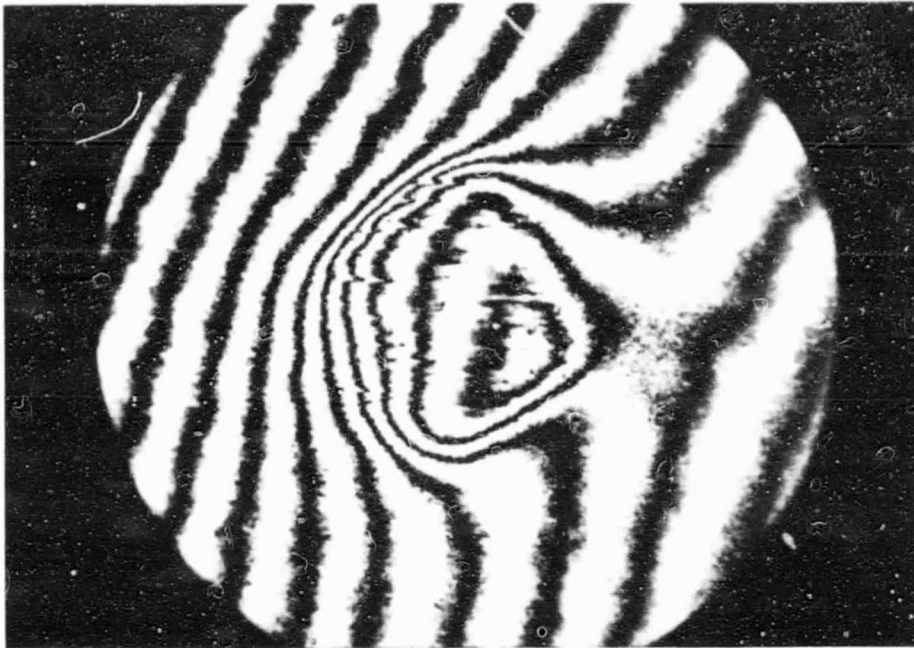
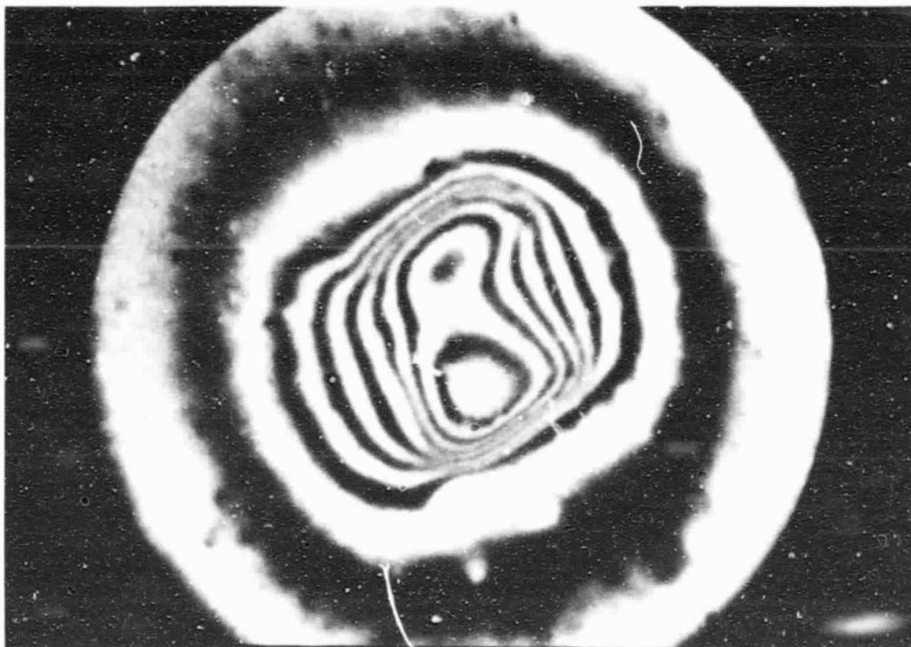


Figure 5.1 - Oxide and defect surface a a typical copy of
the repeating base film asperity on 3M 5198
(400X magnification)



a.



b.

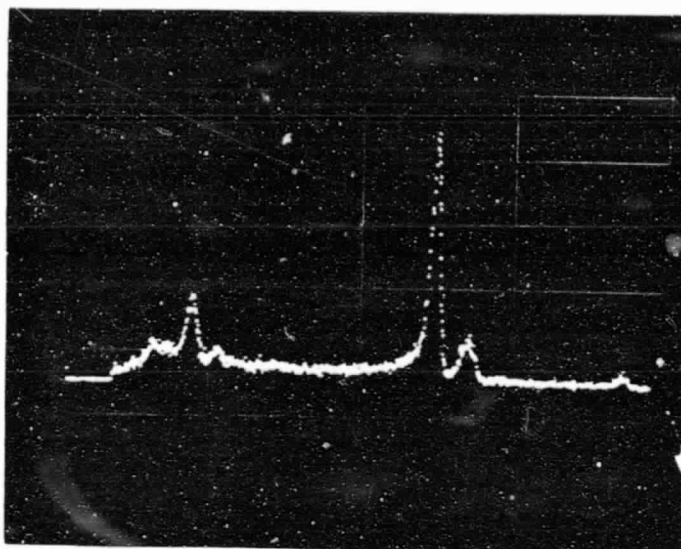
Figure 5.2 - Surface profile at 3M 5198 base film asperity
 a) with oxide binder coating and
 b) after removal of oxide binder coating
 (320X magnification).

narrower than the track, rounded or rectangular signal profiles probably result when the asperity is centered on the track, and more commonly observed bi-lobe profiles probably result from increased head to oxide contact when the asperity is offset from the track center.

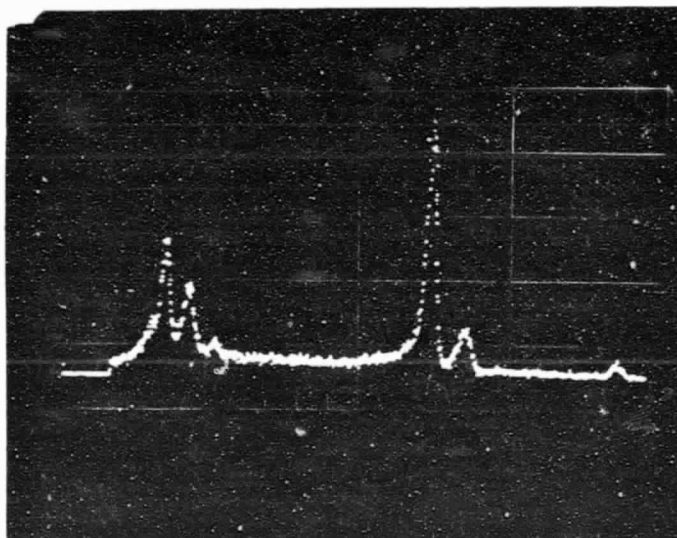
The severity of this type of defect may increase as more base film and surrounding oxide wears away, increasing the area without oxide. This repeating defect could also cause severe head wear leading to premature failure over two or three adjacent tracks. A single occurrence of this type of defect does not suggest that repeating base film asperities are common on 3M 5198, but it is possible that defective base film production equipment has produced the same defect at the same location on other base film webs.

Figure 5.3a is an EDAX spectrum from a normal 3M 5198 oxide binder surface, while Figure 5.3b indicates the effect of a small foreign body inclusion located near defect 3M 5198-35-D. The normal spectrum indicates traces of chlorine and silicon in addition to strong iron peaks, and typical gold and aluminum artifacts. The same elements are detected on both spectra, but the enhanced silicon peak present on the foreign body spectrum suggests a silicon dust particle, while the detection of iron and chlorine can be expected from partial electron beam penetration through the small particle. The size and location of this foreign body was not associated with a 20 dB dropout. These spectra should be compared to other 3M 5198 EDAX results.

One additional interesting 3M 5198 EDAX was obtained from a submicron surface adherent and/or partially imbedded particle which appeared to project 10-20 microinches from the tape surface. The dropout signals that resulted in the identification of this particle were initially classified as permanent, but they actually occurred on adjacent tracks after the virgin recording and the second recording. The particle of Figure 5.4a was found "accidentally" during examination of a more typical deposit that was probably too small or too worn to cause a permanent dropout. The particle was not observed during the defect optical identification procedure. It produced the EDAX spectrum of Figure 5.4b which is high in aluminum but also contains traces of potassium and tin. Probable burnishing agents include aluminum oxides.



a.



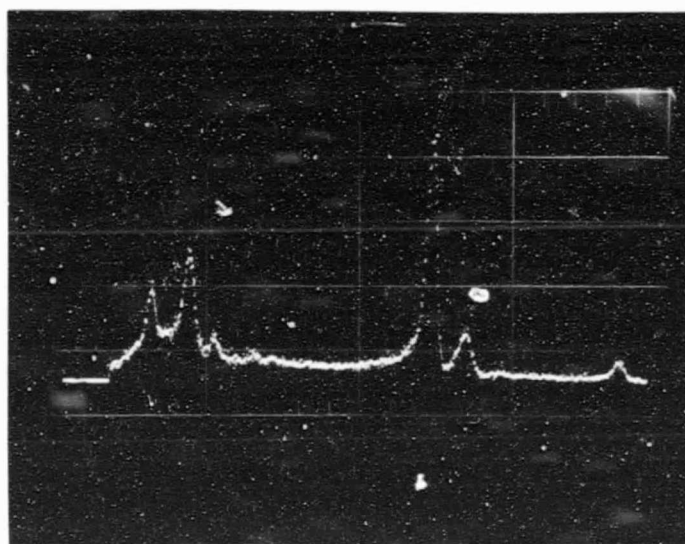
b.

Figure 5.3: 3M 5198 EDXRA spectra of
a) normal oxide surface, and
b) small foreign body inclusion
showing enhanced silicon peak.
The silicon inclusion location
and dimensions were not associated
with a dropout.



a.

ORIGINAL PAGE IS
OF POOR QUALITY



b.

Figure 5.4 - a) SEM and b) EDAX of a small particle located on the surface of 3M5198. This particle was not positively identified as the cause of a dropout.

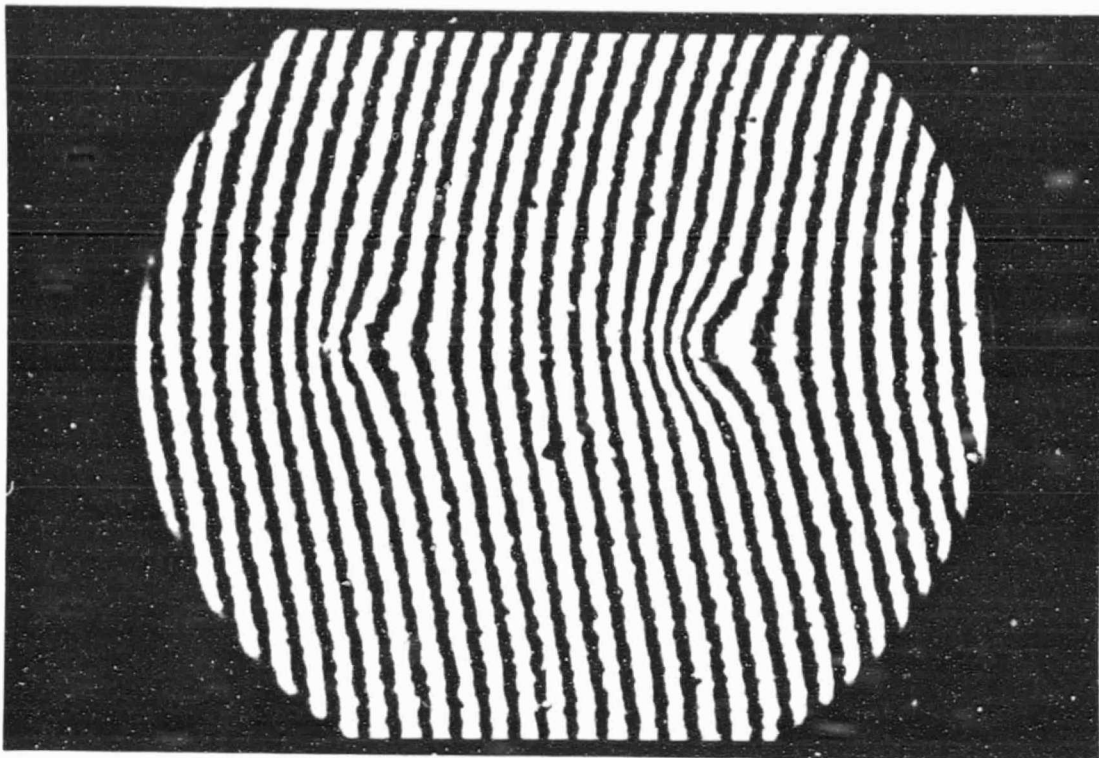
5.1.1 3M 5198 Sample A

The permanent dropouts of 3M 5198 Sample A were located by mapping 8 tracks along a 200 foot tape length. Five permanent dropouts were observed on maps from the virgin recording and the second recording, and the three dropouts spaced farthest apart along the sample were selected for defect identification. One of these three dropouts was in a region where several features were identified, and the defect associated with it could not be determined.

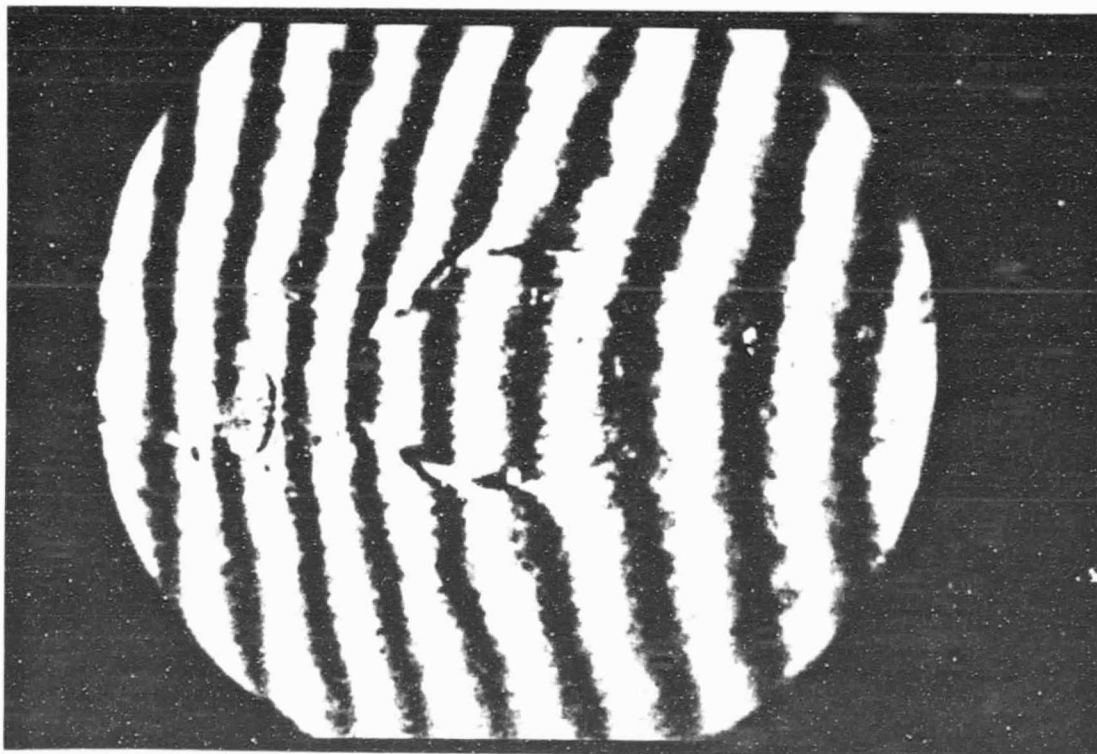
5.1.1.1 3M 5198-40-A

This dropout registered on a single track with a length of 147 wavelengths or 8.8 mils following the virgin recording and 117 wavelengths or 7.0 mils following the second recording. Signal profiles were not observed. A series of similar smooth edged ovoid outlines were observed close to the track center. Smaller irregular masses were present on the take up side of the first and last ovoids in the series, which were separated by 36 mils.

Interference microscopy showed that only the first and last ovoids had significant surface profiles (Figure 5.5a). The profiles do not indicate directly whether the defect projects from the surface or is impressed into the surface, and the profile is too slight to determine its direction from shadowing by oblique lighting. Several features suggest a surface projection. Figure 5.5b shows that the sharp outline of the ovoid with the greatest profile is defined by a narrow ring 3.5 mils wide by 4.5 mils long with a profile in the same direction as the wider overall profile seen at lower magnification. A slight curvature over a large area of the tape surface at the defect was caused by over intense illumination during defect identification and makes the interference band shifts difficult to measure precisely, but the smaller profile is about 5 microinches which may not be sufficient for a 20 dB dropout. The greater profile is estimated at 17 microinches including the 0.4 band interval shift of the narrow ovoid ring. A narrow ring depression would not contribute much to loss of signal, and the width of the defect at the 10 microinch contour is narrower than the track, suggesting tenting by a projection increased the effective width of the defect. The irregular masses observed on the take up side of the two profiles could be material picked up by the heads from elsewhere on the tape and deposited at the projections, but the mass visible on Figure 5.5b may have broken off the ring edge closest to it.



a.



b.

Figure 5.5: Surface profile at defect 3M 5198-40-A. Two prominent profiles are present within 75 mil diameter field of view of (a). Surface curvature away from defects is an artifact. Right feature of (a) is centered in 12.5 mil diameter field of view of (b). Direction of tape travel is horizontal.

The evidence for this defect suggests a series of bubbles in the oxide binder. The two bubbles at either end of the series probably enlarged and broke in the drying oven, forming the measureable profiles, while smaller bubbles between the ends of the series left an oxide surface that was rough enough to be optically observable without leaving a measureable profile.

5.1.1.2 3M 5198-41-A

This dropout was detected on two tracks with lengths of 2.3 mils and 7.3 mils following the virgin recording, and on a single track with a length of 4.4 mils following the second recording. Figure 5.6 is a white light interference photograph of the defect associated with this dropout. The two darkest bands were positioned over the part of the defect that produced the greatest shift which is equivalent to a 50 microinch profile. The main body of the defect is 4.6 mils long and 3.8 mils wide. The irregular outline and the smaller areas of apparently redeposited material on either side of the defect suggest a worn particle adherent to the surface. The defect was not saved after an unsuccessful attempt to measure its tenting effect.

5.1.2 3M 5198 Sample B

This tape sample was 250 feet long and included eight overlapping 7 mil tracks spaced 5.2 mils apart. The first of six permanent dropouts became the subject of the tenting effect measurements, and one additional permanent dropout which had a large size and distinctive signal profile was identified.

5.1.2.1 3M 5198-50-B

The measured length of this dropout decreased from 4.8 mils after the virgin recording to 3.0 mils after the second recording. A dark feature with maximum dimensions less than one mil was affixed to or partially imbedded in the oxide surface at the dropout location. The dark appearance was due to an irregular shape characteristic of mineral dust that prevented direct interference microscopy of the particle. The likelihood of a small fixed surface projection made this defect a good candidate for measurement of the tenting effect.

ORIGINAL PAGE 19
OF POOR QUALITY

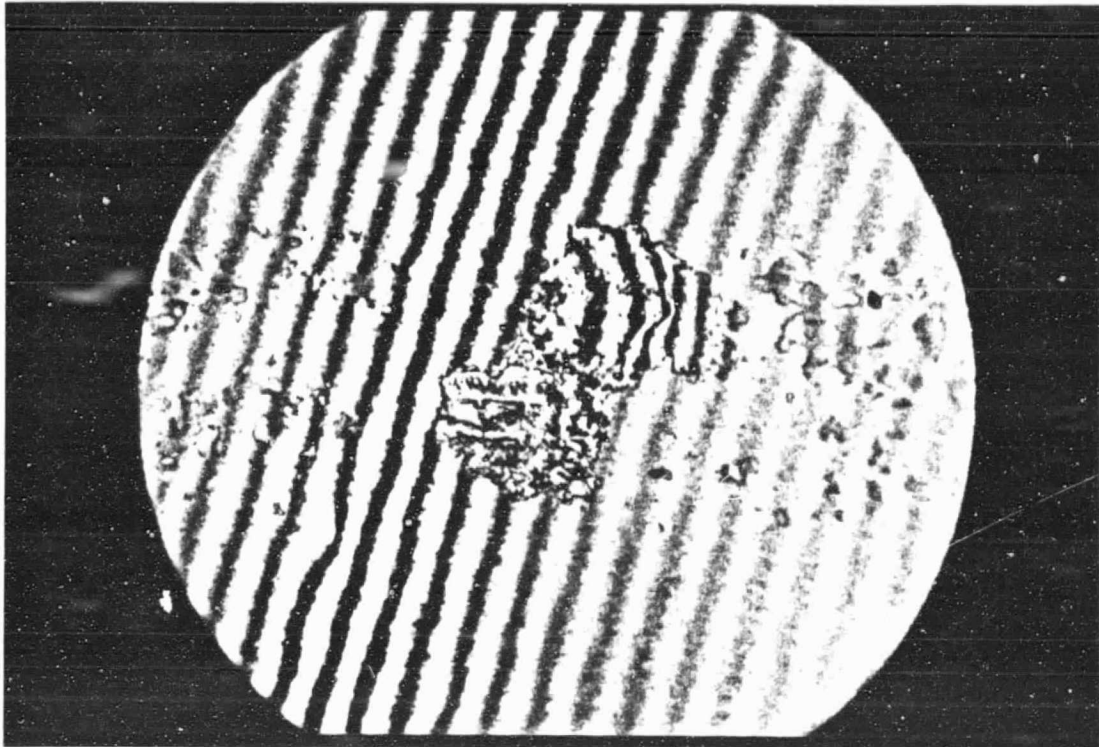
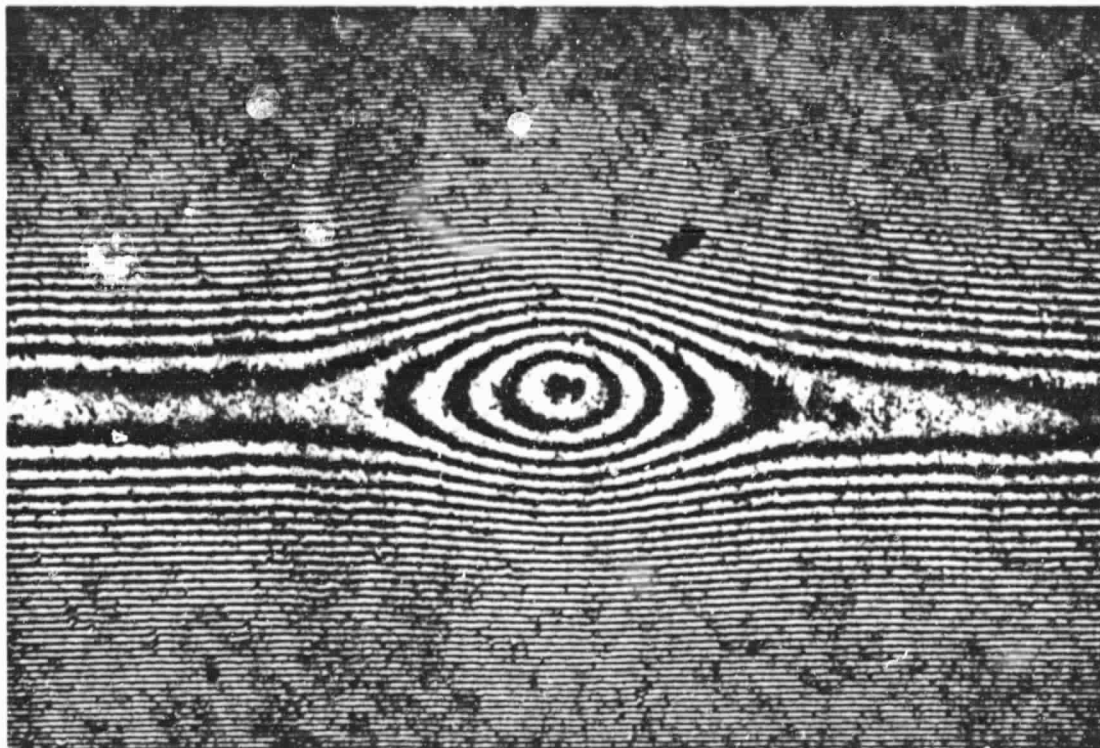


Figure 5.6: White light interference micrograph of defect 3M 5198-41-A within a 12.5 mil diameter field of view. The dark band touching the left edge of the defect corresponds to the narrow sharply curved band over the upper right side of the defect, which is shifted more than 4 band intervals. Direction of tape travel is horizontal.

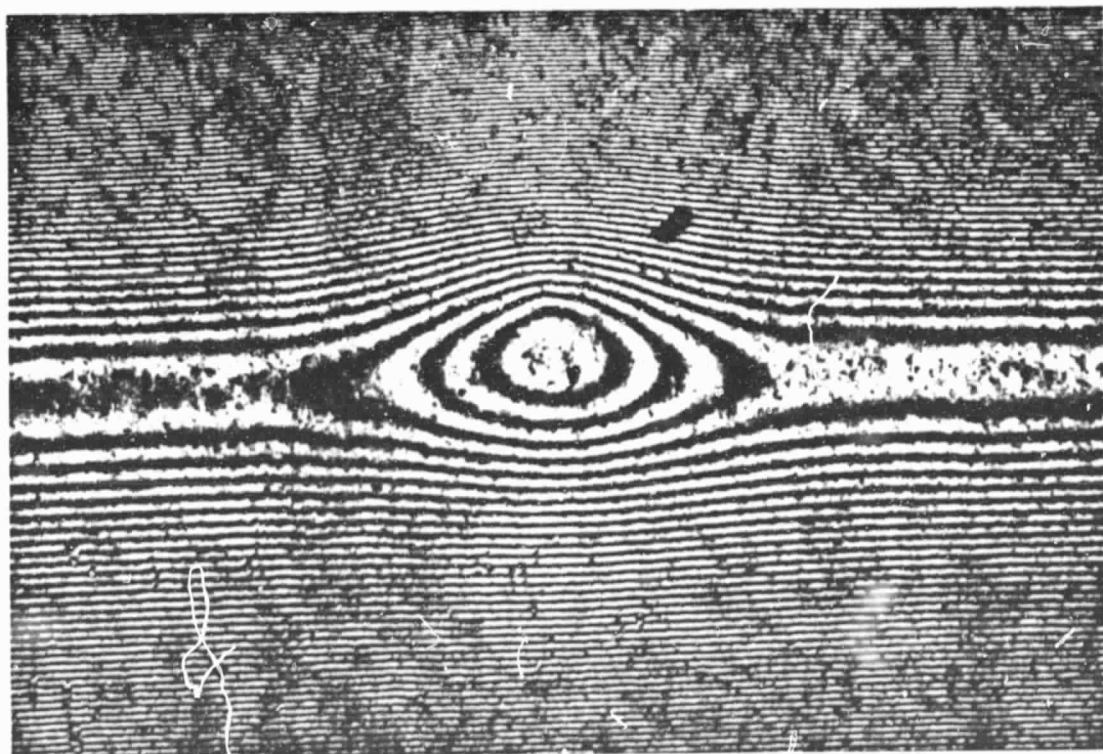
Figures 5.7a and 5.7b are interference micrographs indicating the contours on the back side of the tape with this defect displaced two different distances from the vertex of the glass tubing. The vertex is the widest band and represents the center of the 5.3° wrap or the gap location of the head simulation. For a perfect cylinder, the interference band edges would be straight lines with decreasing separations at greater distances from the vertex until beyond the wrap limit where the separations become constant.

The defect location is the point of maximum deviation of the bands from the horizontal and its displacement from the gap is determined by finding the horizontal line with the greatest number of band crossings and measuring the distance to the vertex at the center of the broadest band. The height of the defect is determined by the number of bands crossed on that horizontal line. Figures 5.7a and 5.7b have defect to gap displacement distances of 3.6 mils and 6.7 mils respectively, with defect heights of 48 microinches and 50 microinches respectively.

Table 5.2 lists measured widths along the gap at four contours caused by tenting at the two defect displacements. Radial distances from the defect to the intersection of the gap and each contour are also listed. Circular contours would produce equal distances for a given line across the table. The measured distances are actually longer for the greater displacement, suggesting elliptical contours, and the distances between contours suggest a gradual change in reproduced signal loss with respect to position along the gap rather than the abrupt effective area assumption of the model. It is likely that the change in record losses would be more abrupt than the slope of the separation distance due to the narrow switching field distributions of oriented particles. It is notable that the dimensions at the 16 microinch contour are much greater than the measured dropout length, while a separation distance of only 10 microinches was estimated for significant combined record/reproduce losses earlier in this report.



a.



b.

Figure 5.7: Tenting effect around defect 3M 5198-50 B. Scale is 9.74 mils/inch. Simulated gap location is along center of widest band, and defect locations (a) 3.6 mils from gap, and (b) 6.7 mils from gap were measured by the technique described in the text.

Table 5.2: Head to tape separation resulting from tenting effect is indicated by contour width measurements along the gap with two different positions of a point defect projecting 50 microinches from the tape surface.

<u>Head to Tape Separation Contour (microinches)</u>	<u>Defect to Gap Displacement Distance (mils)</u>			
	<u>3.6</u>		<u>6.7</u>	
	<u>Width of Separation (mils)</u>	<u>Defect to Contour Distance (mils)</u>	<u>Width of Separation (mils)</u>	<u>Defect to Contour Distance (mils)</u>
5	19.3	10.3	18.9	11.6
11	15.7	8.6	14.2	9.8
16	10.1	6.2	8.8	8.0
21	4.5	4.2	=0.0	6.7

5.1.2.2 3M 5198-51-B

This dropout registered lengths of 8.2 mils, 9.7 mils and 5 mils on three adjacent tracks following the virgin recording, and lengths of 6.5 mils and 4.4 mils and 0.0 mils respectively on the same three tracks after the second recording. Its signal profile with a head position intermediate between the tracks that produced the longest measurements consisted of a deep rectangular loss of signal followed closely by a short sharp profile, a period of near normal signal level, and a shallower rounded profile, all over a period equivalent to a tape length of about 50 mils.

An array of at least three defects were present along 14 mils of the intermediate track position. Most of the defect features had deposit characteristics, but the grainy texture of one smooth 10 microinch profile between deposits indicated a projection of the oxide binder surface and suggested that other oxide binder projections may lie under the deposits at the ends of the defect array. While one of these deposits appeared to be only 5 microinches high and therefore is not likely to cover a projection, a white light interference shift of 3 band intervals was counted on the deposit at the other end of the array which indicates a 35 microinch profile.

5.1.3 3M 5198 Sample C

Larger areas were mapped starting with this sample in an attempt to identify and analyze statistically meaningful populations of defects associated with permanent 20 dB dropouts. As with previous samples, permanent dropouts were selected for defect identification without regard to indicated size, but some judgement was exercised in avoiding closely spaced dropouts to reduce identification ambiguities. Defects 3M 5198-00-C and 3M 5198-01-C were exceptions to this practice. They were separated by one inch along the tape and 60 mils across the tape. Those two defects along with 3M 5198-05-C and 3M 5198-12-C were submitted for SEM and EDAX following the optical examination.

5.1.3.1 3M 5198-00-C

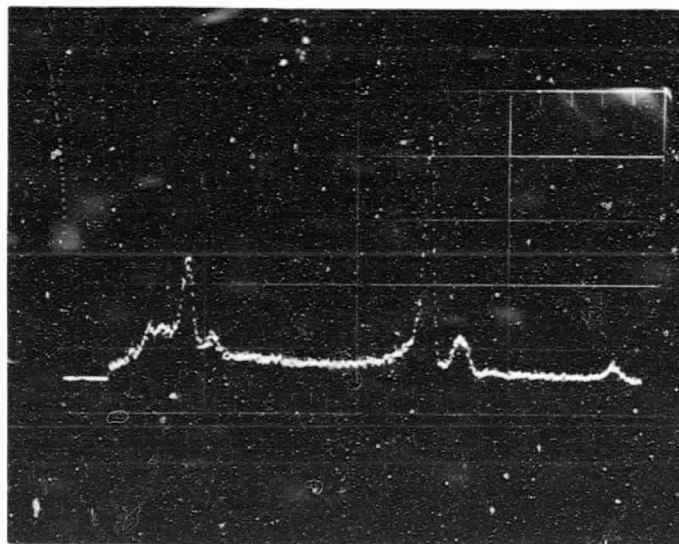
This dropout had lengths of 6.5 mils and 8.1 mils on two adjacent tracks following the virgin recording. It registered a 5.2 mil length on a single track after the second recording. The signal profile was not observed. Optical examination revealed two main areas of material on the tape surface centered between the two tracks that registered counts after the virgin recording. The material was smeared, and smaller deposits were also present along the tracks. The defects were spaced about 28 mils apart along the tape. They were submitted for SEM and microanalysis.

Figure 5.8a is an SEM of the larger particle at this defect, and Figure 5.8b is an EDAX taken over most of the particle area. The lower three-fourths of the particle surface exhibits longitudinal grooves expected for surface wear during passage over the heads, but the smaller deposits and the upper fourth of the main particle have very smooth surfaces. Mechanical contact between practically any solid materials should enable observation of the typical grooved wear surface at this magnification, and the lower profile above the horizontal boundary between the particle areas suggests a reproduce track edge. Thermoplastic deformation (melting) of the particle has been suggested as a cause of the smooth surface. Presumably, heat would be produced by friction between the projecting reproduce head and the tape or defect surface. Note that normal 3M 5198 oxide binder surface including calendar marks never appears worn or deformed after passage of the head.

The EDAX spectrum from this defect is very similar to normal 3M 5198 oxide binder (Figure 5.3a), but the gold peak of the defect spectrum appears slightly enhanced when compared with the primary iron peak. This could result from partial attenuation of the electron beam as it passes through a thin purely organic material to the underlying oxide coating.



a.



b.

Figure 5.8 - a) SEM and b) EDAX of Larger
Feature at Defect 3M 5198-00-C

5.1.3.2 3M 5198-01-C

This dropout affected a single track with an indicated length of 3.6 mils on each of the two dropout maps. It was associated with a long area of surface roughness including one optically observed 4 mil diameter feature centered on the track. Most of this rough area had grainy texture associated with oxide binder. The overall length of the area was 0.14 inches.

No tall projections or wide, deep depressions were evident during SEM, but gradual profile changes can result in very low SEM contrast. The SEM of Figure 5.9 suggests an area of thin surface deposits similar to those seen on Figure 5.8a near defect -00-C. The EDAX spectrum of this area was like normal oxide binder.

5.1.3.3 3M 5198-02-C

This dropout registered lengths of 8.2 mils, 7.9 mils and 8.8 mils on three adjacent tracks following the virgin recording, but only the first of these three tracks indicated a 4.0 mil long 20 dB dropout after the second recording. Optical identification revealed a 1 mil wide by 2 mils long defect typical of adherent surface material with additional material smeared and deposited for 10 mils on either side of the main defect. The profile of this defect was about 20 microinches. The oxide binder was removed at the defect to check for an underlying base film asperity that could have caused redeposition of an oxide binder particle from the head. The underlying base film was normal.

5.1.3.4 3M 5198-03-C

The dropout length caused by this defect was only 0.3 mils following the virgin recording, but the length increased to 1.7 mils after the second recording. Observed signal profiles after the second recording ranged from almost rectangular with a slight return of signal toward the center to sharply bilobed.

A smooth club shaped outline extended 4 mils across the tape width and 1 mil along the tape length at the dropout location. An irregular outline within the thick end of the club shape and a similar adjacent shape were consistent with removal of an oxide particle from a surface impression and its redeposition immediately after the impression, similar to the SEM appearance of defect 3M 5198-12-C.

ORIGINAL PAGE IS
OF POOR QUALITY

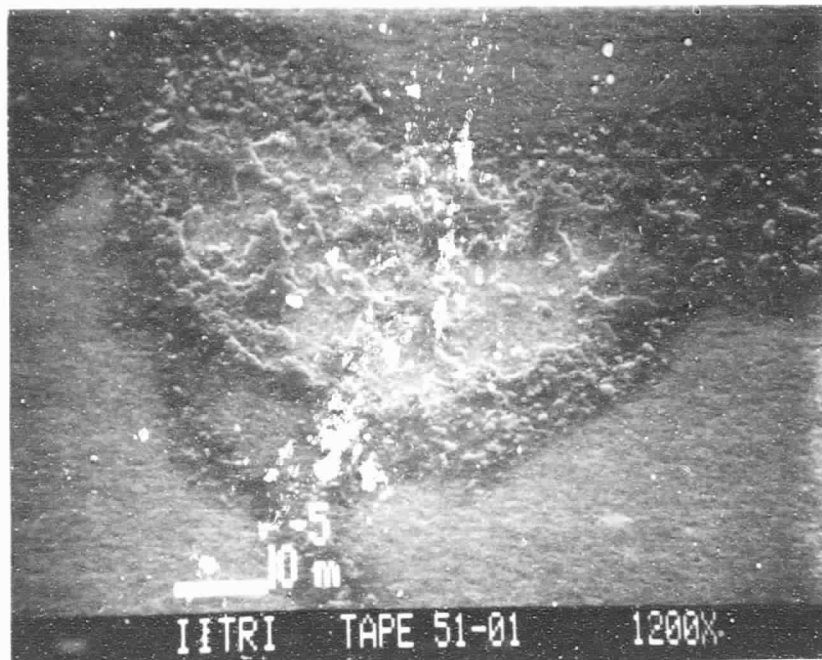


Figure 5.9 - Portion of Rough Surface at Defect 5198-01-C

5.1.3.5 3M 5198-04-C

Lengths of 1.7 mils and 1.6 mils were registered for this dropout following the virgin recording and the second recording respectively, and a triangular signal profile was observed. Optical identification of the defect revealed a 4 mil long crack in the oxide binder with a 1/2 mil diameter deposit at one end. Shadowing indicated a depression on one side of the crack. The crack was perpendicular to the tape travel.

A cuneiform depression up to 40 microinches deep was revealed by interference microscopy. The crack bordered one side of the depression, and the oxide on the opposite side of the crack was elevated about 10 microinches above the level of the oxide binder surface surrounding the defect, which suggests that a projection facilitated the deposit and one end of the crack. The deposit was too small and rough to profile, but the other dimensions suggest that tenting enhanced by the height of the deposit may be responsible for the 20 dB loss of signal. The depression appears to be a mechanically induced gouge, and the overall defect may be correctable by cleaning.

5.1.3.6 3M 5198-05-C

This dropout originally affected three adjacent tracks with lengths of 10.6 mils, 10.8 mils, and 0.5 mils, but only the center track showed a 9.0 mil long dropout after re-recording. Two similar rounded signal profiles were noted which agreed with the identified defect consisting of two smooth edged 4 mil diameter oxide binder surface features separated by 25 mils along the tape length. Material on and around the features suggested secondary deposits transferred by the transport from this pair of surface impression defects. Changes between dropout maps could result from defect wear.

The smooth defect edges disappeared under dark field illumination or SEM, and rough deposits appeared. The varied texture of Figure 5.10 suggests a combination of surface wear and thermoplastic deformation. The EDAX spectrum of this area was like normal oxide binder without an enhanced gold peak.

ORIGINAL PAGE IS
OF POOR QUALITY

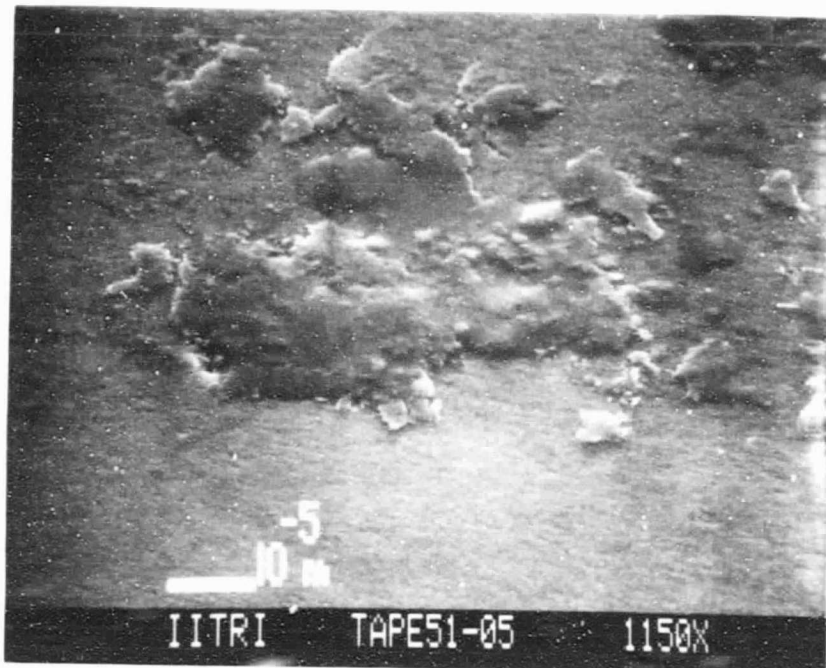


Figure 5.10 - SEM of Deposit at Defect 3M 5198-05-C

ORIGINAL PAGE IS
OF POOR QUALITY

5.1.3.7 3M 5198-11-C

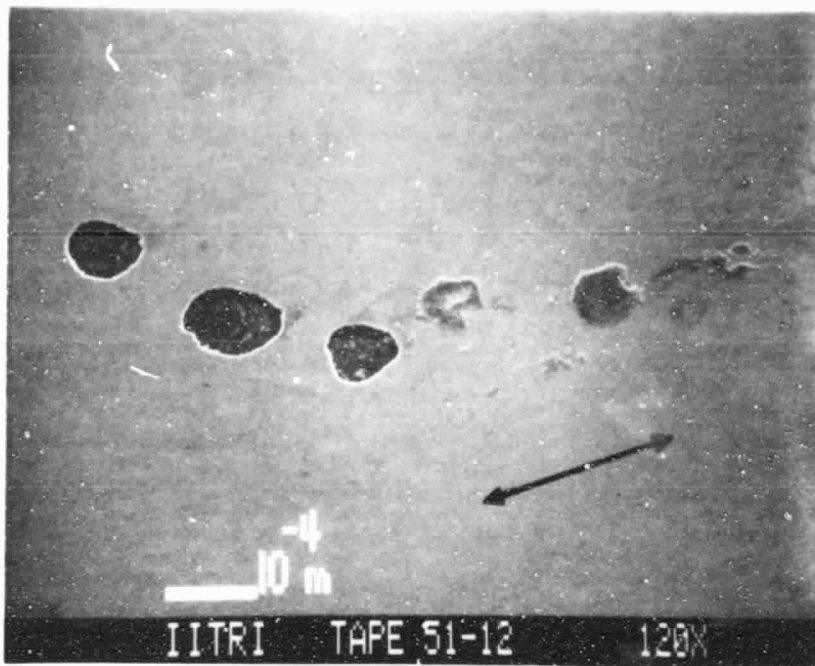
Five adjacent tracks at the location of this dropout had lengths of 15.5 mils, 1.6 mils, 13.3 mils, 5.5 mils and 2.0 mils after the virgin recording, but lengths of 12.1 mils and 4.4 mils on the second and third track alone after the second recording suggest a very unstable dropout or involvement of temporary dropouts along the same 5 foot tape length. The observed signal profile and optical appearance were practically identical with dropout 3M 5198-05-C. The oxide binder at defect -11-C was removed to check for an underlying base film asperity with a negative result.

5.1.3.8 3M 5198-12-C

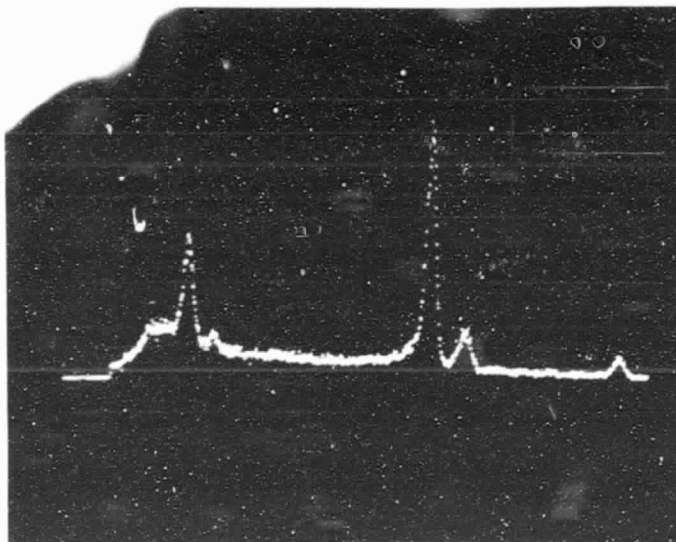
The dropout map from the virgin recording indicated two individual defects separated by one track that did not produce a 20 dB signal depth. Virgin lengths of 7.1 mils and 12.8 mils were recorded, but after the second recording all three adjacent tracks showed 20 dB signal loss with lengths of 3.1 mils, 1.4 mils, and 16.7 mils. Lengths of 3.0 mils and 2.4 mils occurred at the same position along the tape on a track separated from the other three tracks by one dropout free track.

The dropout lengths suggested a large unstable or irregularly shaped defect, and the optically identified defect is consistent with long dropout lengths near the center and guidance sensitive dropout lengths on each end of the defect. A sinuous 50 mil long smooth outline extended diagonally across the tape and enclosed a series of ovoid or irregular features. The ends of the outline were diagonal across the long axis of the tape while the center curved parallel to the long axis. Two ovoids near one end of the ridge had large profiles which were revealed as depressions by shadowing, while the center of the sinuous outline excluding irregular nonreflective shapes had a 15 microinch profile extending upward from the tape surface and therefore constitutes a ridge.

Figure 5.11a is a low power SEM showing that oxide binder has been removed down to the base film at the optically observed depressions, and that the removed oxide binder or other material has been deposited along the tape. The deposits are along the sinuous ridge which does not show clearly in this SEM. Since the individual oxide free areas are less



a.



b.

Figure 5.11 - a) SEM showing three oxide free areas at one end and deposits along center of defect 3M 5198-12-C, and b) EDAX of large deposit closest to oxide free areas. A low profile oxide free ridge encompassing all of the notable features cannot be seen clearly on the SEM, but it extends beyond the field of view on the right side of the image and bears smaller deposits which were aligned with additional dropout tracks. Arrow indicates direction of tape travel.

than 6 mils in diameter (4 mils max.) and the group is less than 15 mils wide, the 20 mil width suggested by dropouts on three adjacent tracks probably results from tenting by the high profile deposits. Slightly smaller features along the ridge which are not in the SEM field of view also had the irregular shapes of deposits and can account for the dropouts on nearby tracks mentioned above.

The EDAX spectrum of Figure 5.11b from the deposited particle closest to the pits has the enhanced gold peak suggestive of material with higher organic content than normal oxide binder, but the SEM strongly suggests that the deposits came from the pits. The deposits do not exhibit worn or smooth surfaces.

5.1.3.9 3M 5198-13-C

Signal reductions greater than 20 dB occurred after the virgin recording on four adjacent tracks at the location of this dropout with 1.0 mil, 15.4 mil, 25.0 mil and 15.7 mil lengths, but only the first, second and fourth tracks exhibited dropouts after the second recording with lengths of 5.8 mils, 6.2 mils and 1.9 mils respectively. Two worn and smeared surface features were observed at the location of the first two tracks while a third feature of similar appearance was present at the fourth track location. Therefore, this dropout includes two or three separate defects which are probably all organic or oxide binder deposits like most of the 3M 5198 defects subjected to microanalysis.

Two of the three features were within 0.25 inches along the tape, while the third feature was 3.5 inches farther along.

5.1.3.10 3M 5198-14-C

Lengths of 2.3 mils and 2.8 mils were measured on a single track following the virgin and second recordings respectively which were associated with a 1 mil wide by 2 mil long area of smeared and worn surface material with the same general features as common 3M 5198 deposits.

5.1.4 3M 5198 Sample D

This final sample was taken to obtain an unbiased sample of permanent dropouts and to obtain additional examples of the deposited surface material type of defect with minimal handling prior to microanalysis. Six permanent dropouts occurred and all six were subject to optical defect identification followed by SEM and EDAX.

5.1.4.1 3M 5198-32-D

This dropout was 10.8 mils and 7.6 mils long on two adjacent tracks after the virgin recording. It was detected only on the second of those tracks with a 13.0 mil length after the second recording, but a new dropout with a 6.8 mil length was detected on the track centered 10 mils before the track with errors after both recordings:

<u>Total Lengths of Dropouts (mils)</u>	<u>Track Location (mils from ref. edge)</u>			
	<u>330</u>	<u>335</u>	<u>340</u>	<u>345</u>
After virgin recording	0.0	0.0	10.8	7.6
After second recording	6.8	0.0	13.0	0.0

A 34 mil long by 14 mil wide area of defects is visible in the dark field illumination micrograph of Figure 5.12, showing three features aligned at 340 mils from the reference edge of the tape and two smaller features near 330 mils, in close agreement with the dropout measurement "image." SEM and EDAX suggested relatively thin worn and deformed deposits with nominal gold peak enhancement shown in Figure 5.13a and b.

5.1.4.2 3M 5198-34-D

This dropout affected four adjacent tracks after the virgin recording with lengths of 8.6 mils, 14.2 mils, 12.5 mils, and 9.1 mils. It repeated on the center two tracks after the second recording with lengths of 15.7 mils and 19.0 mils. The signal profile observed for the 19 mil length track suggested an overall effective length of 40 mils which agrees well with the 35 mil long by 7 mil wide group of smeared surface material identified at the dropout location. Apparently, wear decreased the physical profile and effective width of this defect while smearing increased its effective length between the first and second recordings.

ORIGINAL PAGE IS
OF POOR QUALITY

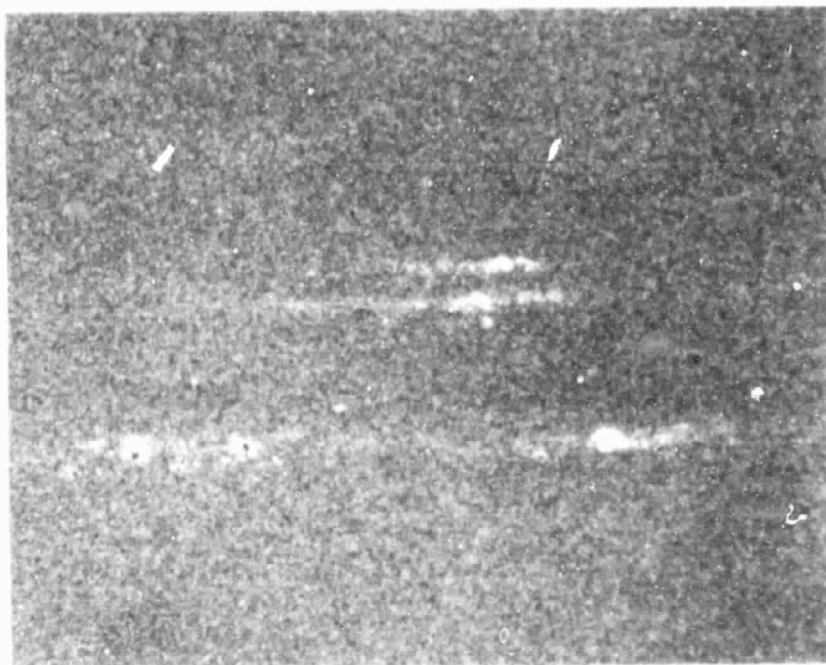
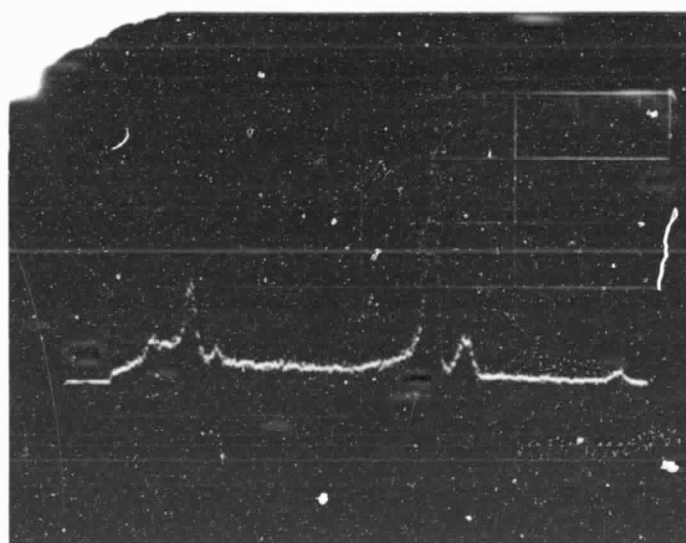


Figure 5.12 - Dark Field Micrograph of Defect
3M 5198-32-C at 82X Magnification



a.



b.

Figure 5.13 - a) SEM and b) EDAX of
One Particle from Defect
3M 5198-32-D

original work to
be published

Figure 5.14 is an SEM of a largest particle from this group and an adjacent smaller particle. Both particles have the smooth surface associated with thermoplastic deformation. The EDAX of the larger particle shown on Figure 5.14b is consistent with oxide binder or thin organic material. The gold peak is not enhanced.

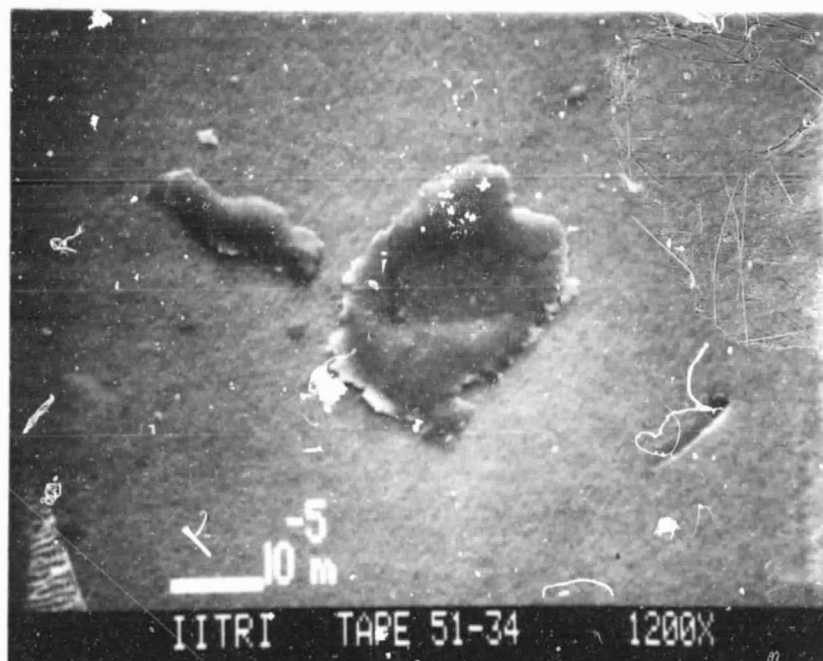
5.1.4.3 3M 5198-35-D

The length of this dropout increased from 2.1 mils on a sample boundary track after the virgin recording to 6.5 mils after the second recording. Its rounded signal profile suggested a defect size or location relative to the track that could be affected by small guidance changes to produce the length changes. A small slightly smeared surface particle was identified as the cause. A typical group of small gouges was aligned over the track immediately on the supply side about 10 mils from the defect.

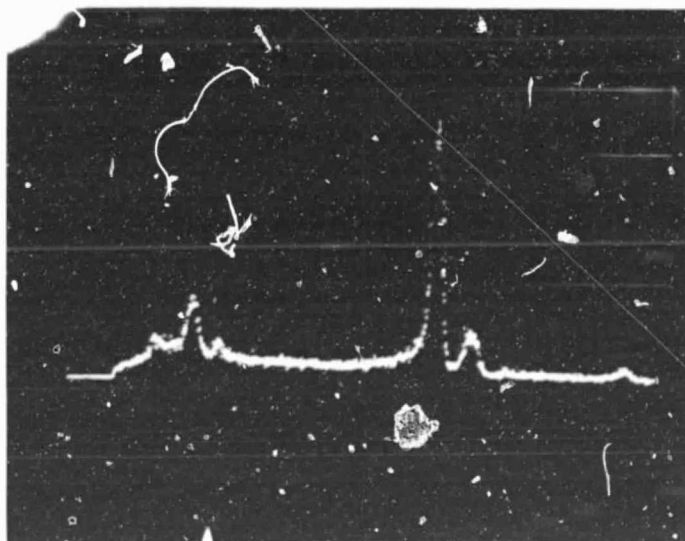
The 1.5 mil long smeared particle on the left side of Figure 5.15 was aligned near the dropout track center. Three members of a gouge array are present on the right side of the image, which corresponds to the supply side of the tape. The dark appearance along the track suggests smearing of the particle material by the projecting reproduce head and passage of the head over the gouges within 20 ms after the defect during observation of the signal profile. A trailing signal profile feature was not observed. Two small pits above the track are an electron beam effect produced during the EDAX of Figure 5.3b, which occurred during point sampling of an 80 microinch long imbedded particle with a high silicon content. Its smooth physical profile and 50 microinch width were not consistent with a dropout.

5.1.4.4 3M 5198-36-D

This dropout length decreased from 7.6 mils and 2.2 mils on adjacent tracks after the virgin recording to 4.2 mils and zero mils after the second recording. Upon identification of the causative defect, a striking similarity to defect -35-D was noted, including approximate size, presence of smearing and/or smaller deposits along the track, and close association with a group of small gouges. A loose correlation was noted between the location of each defect across the tape and the location of the nearest copy of the repeating base film asperity, and profile microscopy of both defects with oxide binder removed is under consideration to check for less severe base film asperities.



a.



b.

Figure 5.14 - SEM and EDAX of Defect 3M 5198-34-D.
 SEM includes one of the largest particles
 among a group that occurred within a
 35 mil long by 7 mil wide area. EDXRA
 of this particle is consistent with
 oxide binder material.

ORIGINAL PAGE IS
OF POOR QUALITY

ORIGINAL PAGE IS
OF POOR QUALITY

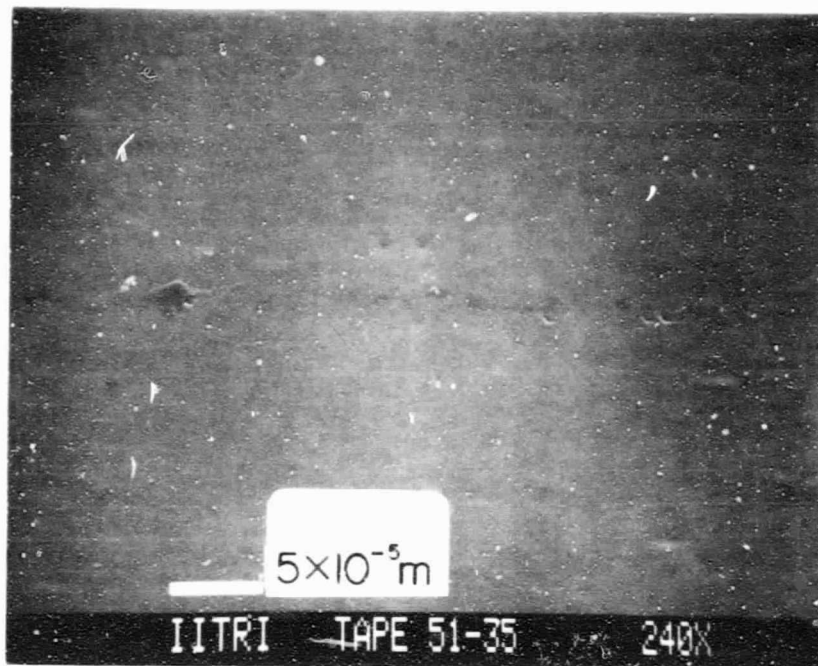


Figure 5.15 - SEM with Defect 3M 5198-35-D at left center and three members of a typical gouge array at right center. Pits above track are electron beam damage that occurred during EDAX of Fig. 5.3b.

ORIGINAL PAGE IS
OF POOR QUALITY

The SEM of this defect in Figure 5.16 shows a particle with a worn surface which distinguishes it from the smooth surfaced defect -35-D.

5.1.4.4 3M 5198-37-D

This dropout had lengths of 8.2 mils on a sample boundary track and 6.0 mils on the adjacent track after the virgin recording which changed to 8.0 mils and zero respectively after the second recording. A rectangular signal profile followed by a narrow triangular subthreshold loss of signal was noted. Optical identification of the defect revealed a smeared deposit and suggested two significant sized particles along the track, but SEM indicated only one major particle with several smaller deposits associated with wear. Figure 5.17 shows the detail of the major particle, which coincides with a reproduce track edge. The EDAX of this defect taken over the thicker worn surfaced upper portion indicated normal oxide binder elements with an elevated gold peak. The lower portion has a much thinner profile and the surface appearance associated with thermoplastic deformation.

5.1.5 Summary of 3M 5198 Results

Eighteen out of the nineteen analyzed 3M 5198 defects include surface deposits among their features. The deposits have different surface textures, but the presence of two textures separated by a reproduce track edge on some deposits demonstrates that surface texture is not a reliable indicator of different deposit materials. The EDAX spectra and the association of deposits with nearby voids in the oxide coating at two or three defects suggests an oxide binder composition. A trend toward higher EDAX gold peaks with thicker defects was noted, but comparison of the slight differences with the particle thickness and the EDAX of Section 5.2.2 shows that the enhanced gold peaks are not strong evidence of oxide deficient binder or pure organic deposits.

The deposits may not be necessary or sufficient for a 20 dB dropout on a 7 mil track in all eighteen cases where they were observed. Two of the deposits were associated with abrupt projections of the oxide binder surface including a bubble induced crater rim and a mechanical gouge. Four more deposits were associated with low profile smooth sided features with the same optical appearance as repetitive calendar defects. Apparently, material



Figure 5.16 - SEM of Defect 3M 5198-36-D

ORIGINAL PAGE IS
OF POOR QUALITY

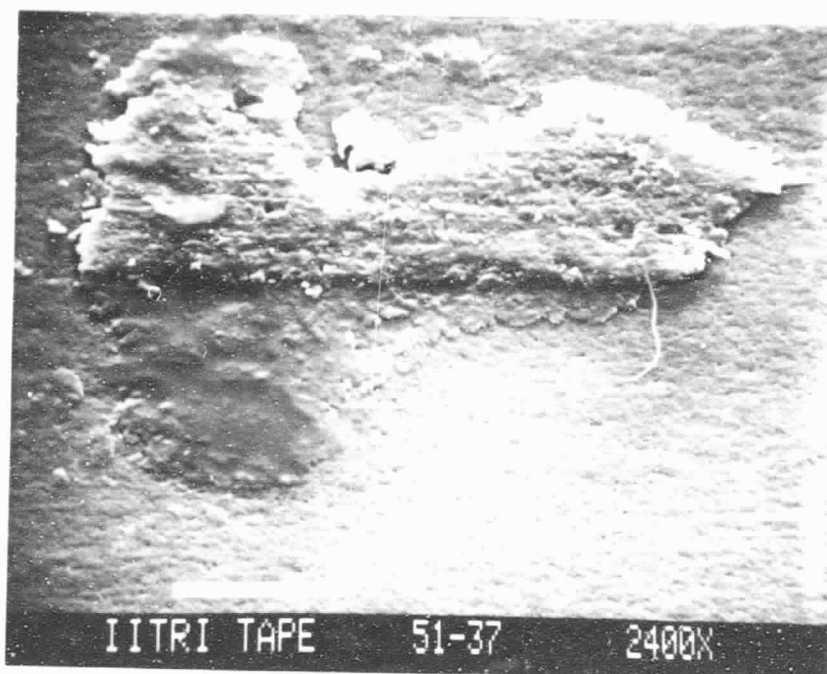


Figure 5.17 - SEM of Defect 3M 5198-37-D

is deposited from the tape to the heads, and any tape surface projection enhances the probability of material redeposition back to the tape. Repetitive calendar marks may appear clean because previous copies of the same mark cleaned the heads before an individual mark under observation reached them.

The observation of deposit defect groups across two or more track widths may be the most significant result with respect to error correction codes. In a few of the analyzed cases, defects or groups of defects were wide enough to simultaneously affect more than one track of an interleaved track headstack, and simultaneous dropouts on three alternating tracks may result from defect 3M 5198-12-C. In two other cases, defects occurred within a length of tape on the order of magnitude suitable for separation of two headstacks. Although neither separation was equal to the 1.5 inch standard IRIG spacing, it seems statistically possible that groups of multiple track defects will occur with spacings that defeat the error reduction benefits achieved by offsetting code frames with interleaved headstacks.

The results suggest that defect types likely to have durable structures are infrequent and do not usually affect multiple tracks. The bubble crater rim of defect -40-A, the imbedded dust particle of defect -50-B, and possibly the gouge of defect -04-C are examples of these infrequent and small defect types.

The deposit type defects and defect groups associated with multiple track dropouts seem to have a less durable nature that could be corrected by cleaning or burnishing, so that the major concern for well conditioned tape would be the lifetime mechanisms and rates of deposit generation, especially at nonrepetitive projections from the oxide binder surface. Defect -12-C is a notable exception to these observations if the mechanism that removed the oxide can function all along the ridge during normal tape usage or if an accelerated wear rate occurs around the oxide free pits.

5.2 Fuji H621 Results

The macroscopic appearance of the Fuji H621 oxide surface is dark and glossy like 3M 5198, but the common microscopic surface features are quite different. The repetitive calendering defects and groups of small gouges present on 3M 5198 have not been observed on Fuji H621. Oxide particle agglomerates are present, but it is difficult to count them because small swales are abundant, and light reflected from these depressions produces variable brightness depending on optical microscope focusing and oxide surface curvature, so that some individual depressions always mimic small agglomerates regardless of focusing.

Maps of two large Fuji H621 samples produced only one permanent dropout indication, and the defect associated with that dropout was not positively identified. The low yield of permanent dropouts indicated on maps prompted abandonment of the mapping technique for the remainder of the Fuji H621 reel. Instead, individual dropouts present after the virgin recording were subjected to a second recording immediately after their initial detection. Some virgin recording dropouts that produced slightly subthreshold signal profiles after the second recording were also considered with the aim of defining the maximum height of a fixed surface projection that does not cause a 20 dB dropout. Therefore, selection of dropouts for Fuji H621 case histories was biased toward smaller and/or less stable defects. A typical result of this procedure was a 25 mil long virgin dropout that reverted to a triangular subthreshold signal profile after the second recording. In one case, imaging before the second recording with track position increments as small as 1 mil showed that the virgin dropout was more than 20 mils wide and produced rounded or rectangular signal profiles, in agreement with the dropout model, depending on the distance between the track center and the defect center as indicated by the longest dropout length. Imaging after the second recording showed that the new subthreshold triangular profile was not due to misalignment between the reproduce track and a small defect.

One set of signal profile observations suggest a loose oxide particle temporary dropout. Two short sharp signal depressions separated by an 18 mil tape length were detectable over a track position range of at least 10 mils with lengths of 1.1 mils to 1.7 mils below 20 dB. This profile did not recur, but a new set of sharp subthreshold depressions separated by a 3 mil tape length appeared after the second recording that could have been caused by the same loose oxide binder particle after deformation or reorientation caused by contact with the heads.

One additional feature of Fuji H621 with possible significance to STR tape life was base film deformation after several passes of the projecting 7 mil head indicating permanent stretching of the base film. An STR with crowned guide rollers could have a similar effect.

Figure 5.18 shows the EDAX spectrum of normal Fuji H621 oxide binder. The indicated elements are similar to 3M 5198 except for the peak at 5.41 which indicates a trace of chromium in the Fuji oxide.

5.2.1 Fuji H621-01

This dropout was 4.8 mils long after the virgin recording and exhibited a stable rectangular signal profile that did not extend to 20 dB following re-recording. The dropout model predicts that the bottom of rectangular signal profiles will correspond to the noise level so this subthreshold profile does not agree with the model. Figure 5.19a is a bright field photomicrograph at the associated defect suggesting a 2 mil long by 1 mil wide area of surface wear which could be deposited material surrounded by a narrow grainy broken ring that is brighter than flat oxide binder. A smaller deposit along the track is also suggested.

Figure 5.19b is the interference photomicrograph of this defect indicating a departure from the smooth normal oxide surface that starts at the outer edge of the light ring. Deflection of the bands in the same direction as swales indicates a depression surrounding a center with a sharp profile transition of indeterminate direction. A depression is also indicated near the smaller optical feature.

ORIGINAL PAGE IS
OF POOR QUALITY

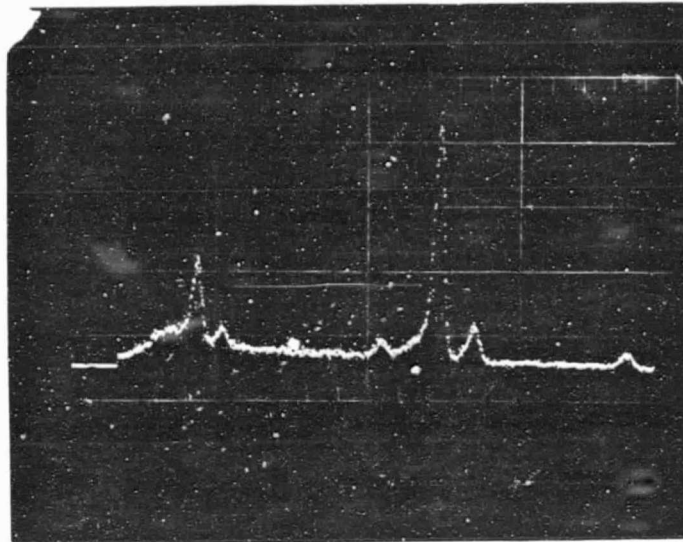
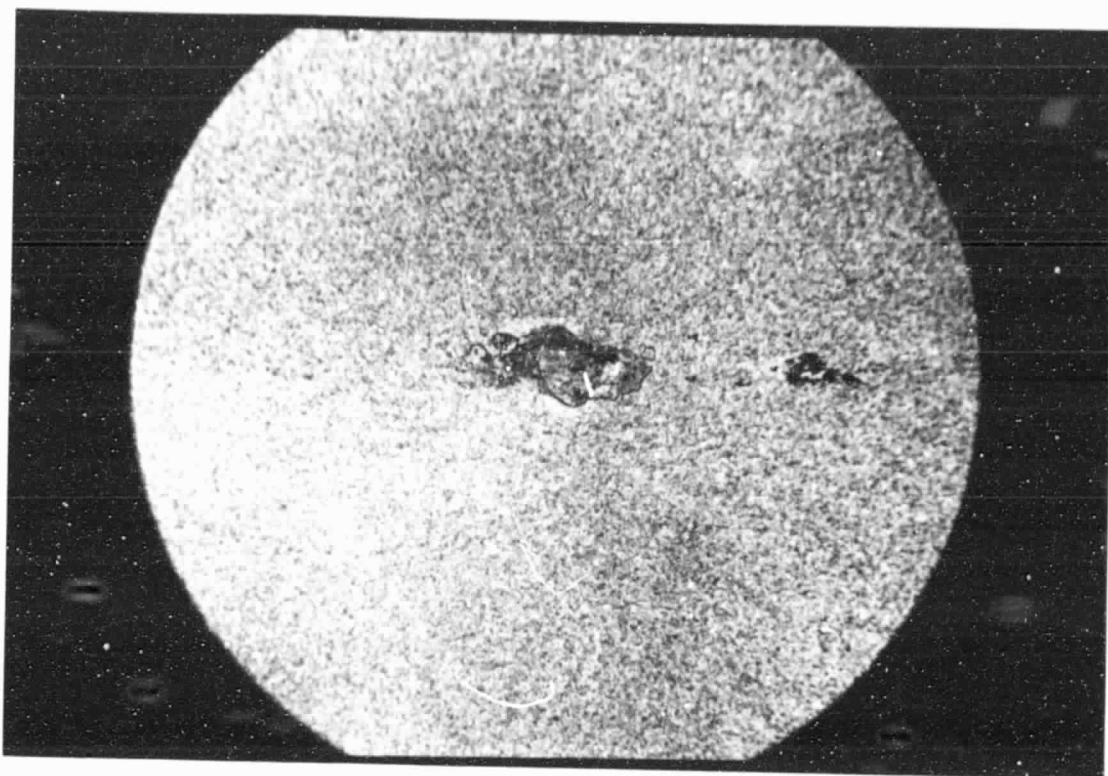
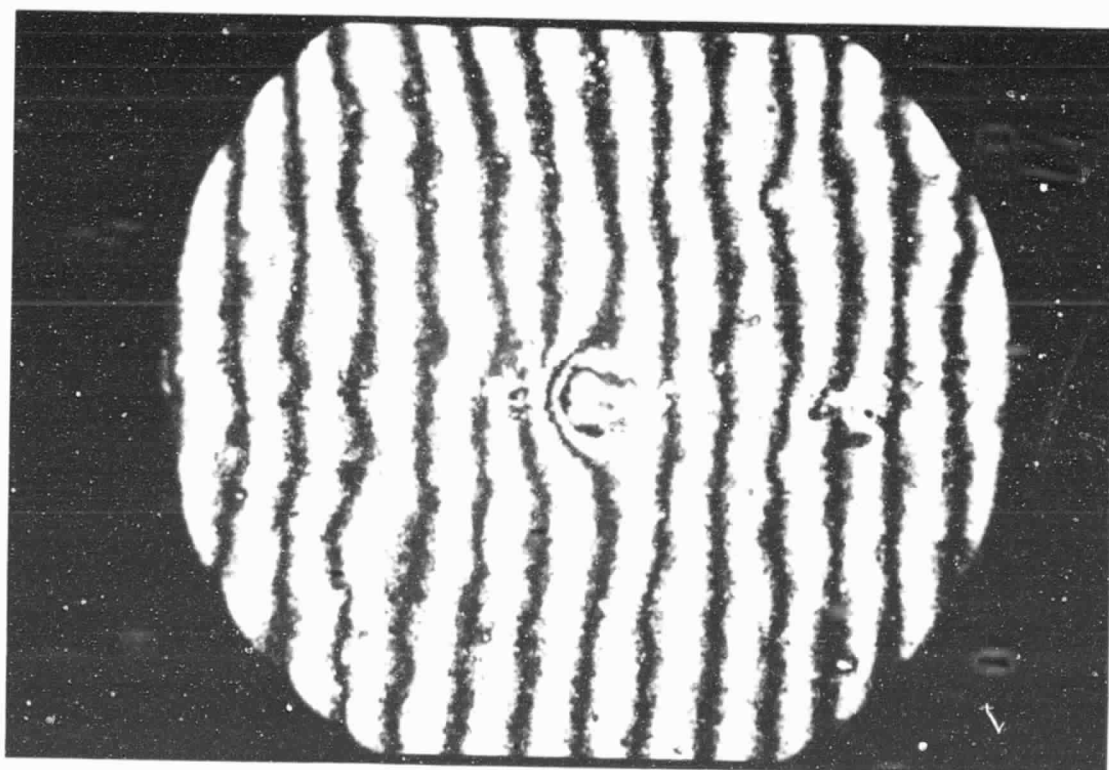


Figure 5.18: EDAX of Normal Fuji H621
Oxide Binder



a.



b.

Figure 5.19 - a) Bright field micrograph and b) Interference micrograph of defect Fuji H621-01 (360X magnification).

The SEM's of this defect in Figure 5.20a and b show a system of surface depressions which partially surround normal or slightly elevated oxide binder. More important, two apparent inclusions project from the surface between the depression systems. The EDAX spectra of Figure 5.21a and b indicate traces of silicon sodium and nickel in addition to a greatly enhanced chlorine peak in the large inclusion, and aluminum, silicon, potassium and calcium in the small inclusion. Additional debris adherent to the surface was not distinguishable from oxide binder.

The gold deposition during SEM preparation of this sample enhanced its reflectivity, enabling more detailed observations with the interference microscope. A maximum depth of 60 microinches was measured at the depressions, and the oxide binder surfaces between them were at the normal level rather than slightly projecting. The inclusions were too small and rough to profile with certainty by interference microscopy, but the SEM appearance compares favorably with the two band interval shift (24 microinches) suggested during the attempt to profile the larger inclusion. Removal of other inclusions upon contact with the heads is a possible mechanism for formation of the surface depressions. If the remaining inclusions and nearby debris deposits could be worn or removed by tape cleaning, the resulting width of all depressions would not merit serious consideration as a potential dropout source.

5.2.2 Fuji H621-02

The dropout associated with this defect was noted once while imaging a nearby dropout during the virgin recording. The dropout counts at the same location after the second recording led to the localization and identification of a highly reflective 2 mil long feature that was centered just off the track positions employed in its detection and the other imaging procedure. The surface of the feature was too rough for profile microscopy.

Figure 5.22a is an SEM indicating a particle resting on the oxide surface. However, the defect was adherent enough to resist an air jet dusting during sample preparation, and review of its detection suggests that it never passed over the projecting reproduce head. A projecting profile between 50 and 100 microinches is suggested. The EDAX of Figure 5.22b is mostly gold and aluminum artifact with minor iron and chlorine peaks from the underlying oxide, which is indicative of a purely organic material.



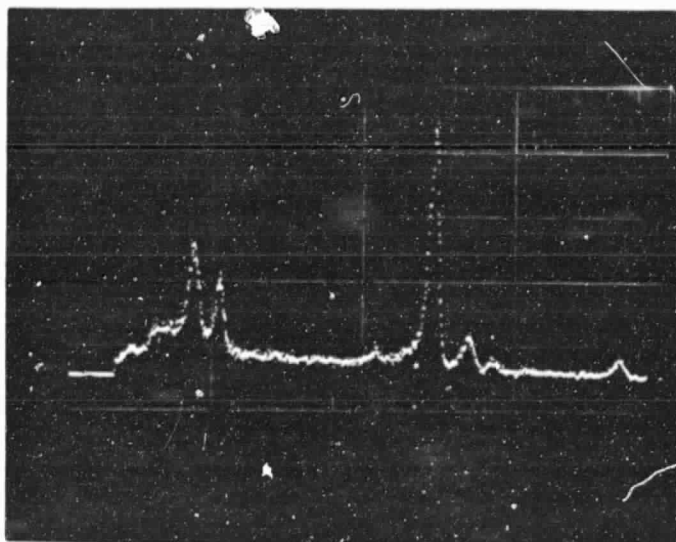
a.



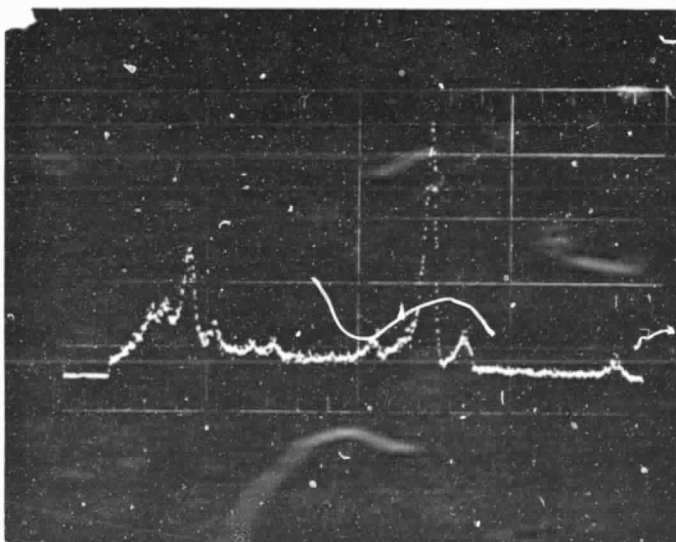
b.

Figure 5.20 - SEM's of Defect FH621-01

ORIGINAL PAGE IS
OF POOR QUALITY



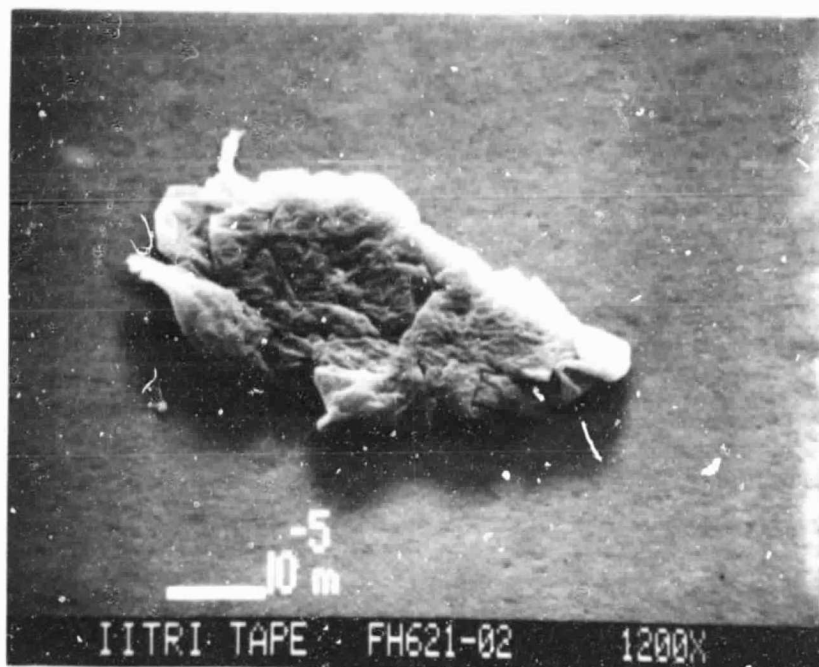
a.



b.

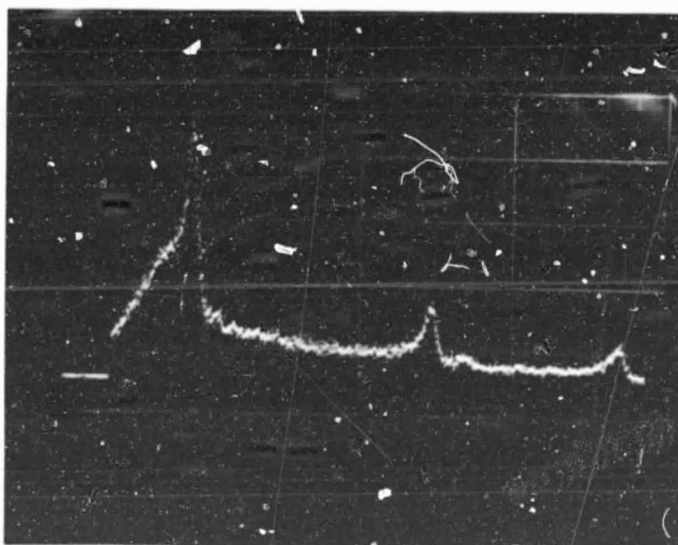
Figure 5.21: EDAX of a) large inclusion and
b) small inclusion of defect
Fuji H621-01.

ORIGINAL PAGE IS
OF POOR QUALITY



a.

ORIGINAL PAGE IS
OF GOOD QUALITY



b.

Figure 5.22 - a) SEM and b) EDAX of
Defect Fuji H621-02

Comparison of this defect with those on a heavily contaminated section of another Fuji reel is under consideration.

5.2.3 Fuji H621-03

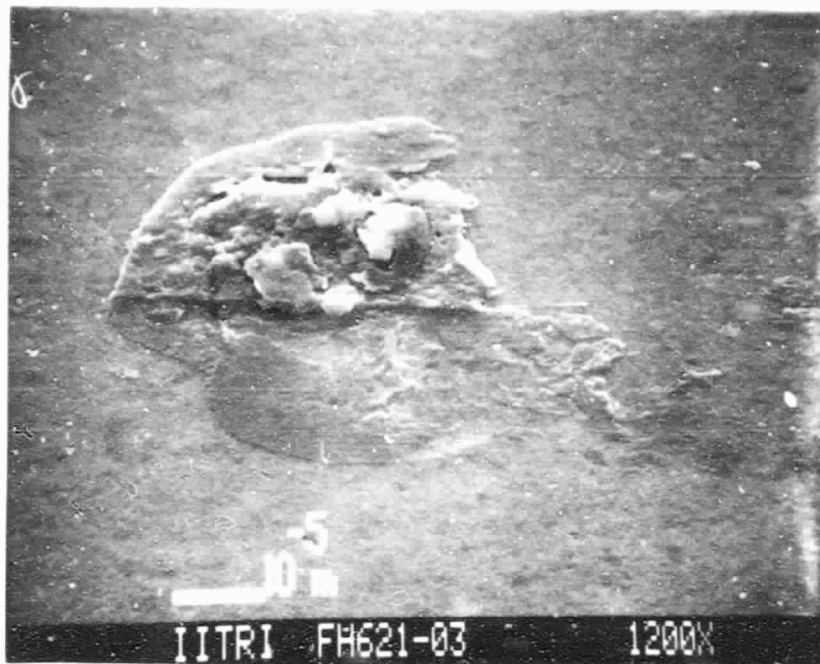
This dropout was 6.6 mils long during the virgin recording and exhibited a rectangular signal profile followed closely by a 6 dB triangular profile. A similar profile was noted at the defect location after re-recording, but the loss of signal did not exceed 20 dB. A worn surface defect about 2.5 mils in size centered about 4 mils from the track center was present at the dropout location. The optical appearance suggested wear and much smaller redeposits along the tape travel direction a few mils from both sides of the main defect which could approximate where head to tape contact was re-established after passage of the defect and could also account for the trailing signal depression. The defect surface was too rough for interference microscopy.

Figure 5.23a is the SEM of the defect showing worn apparently soft material surrounding cubic crystalline shapes with the highest profiles. A track edge offset from these high profiles is suggested, and partial recording over a wide tent with good reproduce head to tape contact after the second recording readily accounts for the dropout measurements.

Figure 5.23b is the EDAX from a large area of this defect indicating enhanced potassium and chloride peaks in addition to normal oxide binder elements. Therefore, the defect is almost certainly KCl crystals embedded in an oxide binder or thin purely organic deposit. The evidence does not indicate if projecting crystals facilitated a redeposit from the head or if crystals and oxide/organic material were deposited simultaneously.

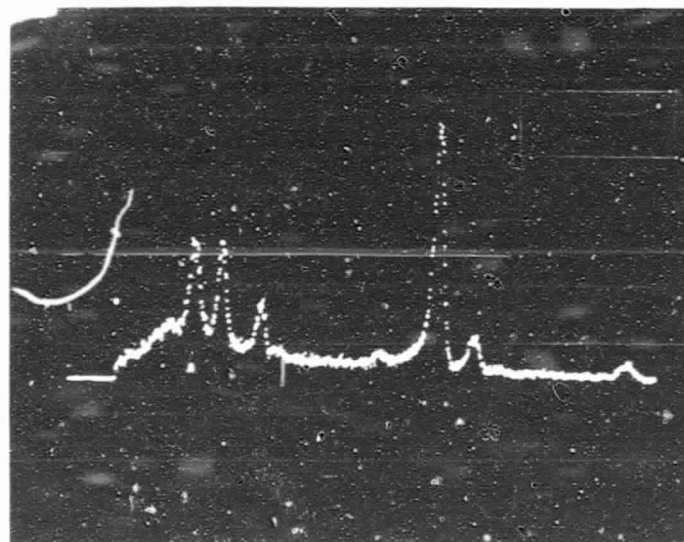
5.2.4 Summary of Fuji H621 Results

None of the three Fuji H621 dropouts that were subjected to defect identification and analysis can be considered permanent according to the strict definition and controlled test conditions employed for 3M 5198. Two of them exhibited subthreshold signal profiles after the second recording, while the physical defect structure associated with the third dropout was probably not subjected to the changes induced in other defects by contact with the projecting reproduce head.



a.

ORIGINAL PAGE IS
OF POOR QUALITY



b.

Figure 5.23 - a) SEM and b) EDAX of
Defect Fuji H621-03

The temporary nature of most Fuji H621 dropouts may result from movement of relatively hard, nonadhesive particles through contact with heads. Individual components of all three identified defects are consistent with this hypothesis, and the projecting points of oxide binder inclusions or the association of crystalline contaminants with softer material could well be infrequent exceptions to typical Fuji H621 defects. The significant results of this study include the indication of a few wide dropouts that might defeat an error correction code and the permanent base film stretching caused by the reproduce head. The temporary nature of the wide dropouts prevented analysis of their associated defects. At this point it seems more valuable to determine if the wide defects can be reduced by conditioning and cleaning, or if wide defects are being removed by the heads and generated by redeposition or other mechanisms simultaneously.

6.0 CONCLUSIONS AND FUTURE DROPOUT MEASUREMENTS

This section includes plans and possibilities for further defect analysis, extended use dropout measurements, and analysis of those dropout measurement results with respect to code formats and error correction capabilities. Many of the plans and suggestions are based on conclusions reached from results in the current report and during previous work. These conclusions are presented or repeated at points appropriate to the discussion of the future measurements and analyses.

6.1 Dropout Dimensions and Distribution

Suitable HDDR codes should be able to detect and correct the long strings of lost data on at least one track that results from typical defects. Although some dropout lengths appear to increase due to smearing of the causative defect along the track, the maximum lengths encountered in this study were not associated with intractible error generation. The maximum dropout lengths of 1000 bits from 3M 5198 and 1200 bits for Fuji H621 indicated on Figure 4.5.3 of Monthly Reports 8-11 could have resulted from more than one defect on a given track within a 10 foot tape length, but those lengths should be employed as a conservative estimate of worst case lengths.

A typical HDDR code cannot correct data lost by simultaneous dropouts on more than two tracks of a 16 track code block, and offset code frames resulting from interleaved headstacks provide immunity from large defects that affect four adjacent tracks simultaneously. With a greater number of narrower tracks, several code blocks can be interleaved across the tape width, providing the same level of immunity from single large defects as the lower density 16 track system. The results in Section 4.5.1 of Monthly Reports 8-11 suggest that dropouts are isolated, more or less randomly distributed events along the length of a tape, which implies that simultaneous dropouts resulting from more than one track should be rare. However, one Fuji H621 result from Section 4.4.1 of that report was an obvious nonrandom longitudinal distribution of defects, and current 3M 5198 results demonstrate the occurrence of defect arrays. In some cases, the defects are oriented across the tape width. These results and the HDDR code considerations mentioned above suggest that the occurrence of

simultaneous small dropouts rather than single large dropouts may be a limiting factor in the performance of the subject tapes. Simultaneous multitrack detection has not been possible with the single track 7 mil head employed to obtain data for this report. The multitrack head expected from RCA should enable measurement of this critical parameter.

Many defects are present that did not cause 20 dB dropouts on a 7 mil track, and the frequency of occurrence decreases as the size of defects increases. Surface depressions may be as common as projections of equal physical size, but tenting around projections greatly increases their effective size, and 20 dB dropouts are caused by projections at most or all of the analyzed defects rather than by the depressions associated with several of the defects.

The 3.6 mil defect to gap distance during the tenting effect measurement closely simulated half of the measured dropout length and produced a head to tape separation of about 20 microinches across the track width. The slightly diminished head to tape separation measured for the 6.7 mil defect to gap distance suggests a lower limit for the head to tape separation that results in 20 dB loss of signal. The defect for the tenting measurement was 50 microinches high and was much narrower than the track. The accurately measured physical heights of narrow deposit defects suggests that an even lower head to tape separation distance can cause 20 dB loss of signal. However, defect wear and deformation during dropout measurements due to the projecting reproduce head along with uncertainty of the precise head to defect alignment subjects these inferences to error.

Optical defect dimension measurements provided confidence in several of the defect identifications and helped to eliminate calendaring impressions as a typical source of 20 dB dropouts. They will be continued as required on a case by case basis. SEM results showed that the smallest projecting inclusions may not be observable optically, but their apparently isolated distribution and the small dropouts that result from them should be the easiest problem to deal with by using error correction codes and offset frame formats.

6.2 Surface Defect Analysis

The results in this report provide a good sampling of 3M 5198 defects and point to some particularly significant types. Identification of defects associated with Fuji H621 dropouts was less successful, in part due to their lower frequency of occurrence, but also because their physical structure or location changed in response to the test conditions and techniques. These conditions actually concentrated efforts toward the identification and analysis of more significant defect types, and an investigation of 3M Type 973 and Ampex Types 466 and 721 employing the techniques in this report is planned before proceeding with the dropout measurements during extended tape use. Applying the experience gained in the current study may reduce the level of effort required for significant results from those tape types.

Quantitative results from small particle analysis become increasingly difficult as the size of the particles is reduced. However, EDAX results indicate that common 3M 5198 surface deposits are almost certainly oxide binder. EDAX and SEM suggest silica dust and aluminum oxide for the inclusion and projecting particle of 3M 5198 which were not associated with dropouts. The aluminum particle may be the result of sapphire or another corundum burnishing agent employed by 3M during the production to reduce the more common deposits and impressions.

Fuji defect materials include an unidentified purely organic particle and mineral particles including light metals, nickel, tin and potassium chloride. Oxide binder or an unknown organic appears to be involved with the potassium chloride defect.

Laser micro Raman spectrometry with a molecular optics laser examiner (MOLE) is under consideration for further analysis of these defects. Like conventional IR spectra, Raman spectra are complex and are best used as fingerprints for comparison with spectra of known materials. The availability of known Raman spectra is much more limited than IR spectra and offer little hope of identifying the chance organic contaminant. Of course, known spectra could be prepared for oxide binder, base film and back coating which could lead to positive identification of the common materials involved in the defects described in this report. For analysis of unknown

materials, defects should be removed from the oxide surface prior to MOLE, and the sizes of defects described in this report approach the limits of sample micromanipulation capabilities. Another potentially useful MOLE capability is the selective imaging of known materials present in a defect with a complex structure.

Common defect materials on both tape types including the defect groups on 3M 5198 can be worn, moved and/or removed from the tape, and further study of those aspects may be more productive than attempts to identify materials with the hope that the underlying defect sources can be determined and eliminated.

Two of the defect types identified on 3M 5198 are of particular concern, and future studies will include attention to the detection and identification of more defects like them. The obvious potential problems associated with the repeating base film asperity have been discussed, and defects of this type can be detected and analyzed easily. Defect 3M 5198-12-C involves an oxide binder ridge which could be similar to common calendaring impressions. Its appearance suggests the possibility of accelerated localized tape wear that could quickly affect several tracks by spreading along a calendaring impression. Future identification of this defect type will only require optical microscopy and can be conducted at the end of an extended use dropout measurement series. Additional defect material analysis mentioned above may be employed to determine if the ridge, pits, and deposits of this defect resulted from organic inclusions rather than an accelerated wear mechanism that could occur at any calendaring impression.

The identified Fuji H621 defects are small and should be handled easily by error correction codes. Once again, low dropout rates indicate a clean high performance product which serves as the standard for comparisons with other tape types. Future measurements will include the rate of debris generation and possible degraded performance with extended use. Opportunities to identify the source of large temporary dropouts on Fuji H621 will be sought, and white debris on a heavily contaminated section of Fuji H621 may be analyzed. The implications of the permanent base film deformation observed after dropout measurements on Fuji H621 must be considered with respect to STR applications.

6.3 Measurement of Dropout Performance During Extended Tape Use

An indication of lifetime dropout performance and debris generation is essential to the selection of the best tape type for the STR application. The beneficial effects of conditioning on new reels of most tape types is a well known phenomenon which is routinely employed by HDDR system developers before attempting BER measurements. Although dropout measurements on virgin tape provide useful benchmarks for lifetime analysis, results from conditioned tape are certainly more representative of actual performance during use than measurements on virgin tape. A series of dropout performance measurements alternating with cycles of tape conditioning is planned to determine the magnitude of initial improvement and to investigate degradation of performance after the limit of improvement is reached. Tape conditioning will include shuttling over dummy heads, initially with a standard protocol for speed, tension, number of passes, and dropout measurement frequency. Variations of the protocol may be introduced if initial results suggest more productive techniques.

Occasional tissue cleaning of oxide surfaces during initial conditioning requires little additional effort and should accelerate the initial period of improvement. Cleaning will also provide rapid qualitative indications of oxide binder debris present on virgin tape and the rate of debris generation. Current results suggest that tape conditioning and cleaning may also lead to economical procedures for postproduction improvement of tape reels prior to their installation in an STR. Blade cleaning techniques are also under consideration, but this more radical test variable is not planned during the next measurement series.

Once the limit of performance improvement is reached, cleaning will be suspended, and the conditioning protocol will be changed to simulate as closely as possible the conditions anticipated for actual use of the tapes in STR's. However, a tissue sample from the cleaning of a tape after the final dropout measurement can be ashed and weighed to provide a quantitative measure of oxide binder debris generation when results indicate that this mechanism is a problem. Defects associated with large permanent dropouts will also be identified and analyzed at this point.

6.4 Heads Selection & Data Analysis

The effect of the currently available 7 mil reproduce head on defects may exceed cleaning and conditioning effects, and multiple pass measurements are not accurate enough to distinguish simultaneous dropouts caused by multiple defects, so this head cannot be considered for the extended use investigation. The original 18 mil 42 track head was delivered with very few functional tracks, but its replacement is expected soon from Honeywell. The defective 7 mil track head with several functional tracks expected from RCA is probably the best choice for extended use measurements that include coincident dropout detection because less extrapolation of data and less analysis software development effort will be necessary. However, final head selection may be limited to availability following completion of the surface defect analysis on the Ampex tape types, and alternatives to software development have been considered.

With the 7 mil head, only the 20 dB threshold would be required, but with either head, several tracks spread across the tape should be monitored. With this arrangement, uniform random distribution of defect locations across most of the tape width would be assumed, but higher dropout rates likely near edge tracks would be detected at rates proportional to their distribution. The ultimate weight placed on the simultaneous detection results for tape selection depends on the format and code capabilities employed for the STR.

In order to eliminate software development, the dropout detector outputs could be connected to an analog adder constructed with operational amplifiers, and coincident defects could be classified and counted at a few different degrees of severity with comparators connected to the adder output. With this scheme, defect groups above one level of severity would still be mapped along the tape, but not across its width. Counts of lower class defects and defect groups would serve as indicators of debris generation.

If an 18 mil head is employed for the extended use dropout measurement system, the lowest threshold employed to detect the dropouts should approximate the sensitivity of 7 mil heads to the smallest defects that can prevent recovery of data before error correction. A 3.74 dB dropout

detection threshold on an 18 mil track was specified in Section 2 as equivalent to a 20 dB threshold on 7 mil tracks when measuring lengths of case I dropouts. Few of the smallest dropouts would have the alignment for 20 dB loss of signal on 7 mil tracks, and precise measurement of equivalent lengths have little bearing on error correction, so this lowest proposed threshold will be rounded to 4 dB.

An 18 mil track actually covers about three 7 mil tracks, and analysis of data should only consider one of the parallel code systems that will probably be interleaved across the tape to achieve immunity from large defects, so defects that trigger only the lowest threshold should be assigned a low probability of contributing to a coincident multitrack event. Higher probabilities can be assigned to higher thresholds, including 100% for a 20 dB threshold on an 18 mil track.

Current results indicate that the use of a 4 dB threshold with an 18 mil track for the detection of the smallest defects will also detect the numerous wide low profile calendaring impressions on 3M 5198, which could constitute a serious source of error because they cover entire tracks and produce similar short shallow signal profiles on both 18 mil and 7 mil tracks by a mechanism similar to the one assumed for curve C of Figure 3.1. Since error correction codes suitable for HDDR applications must handle burst errors, the precise length data from dropout measurements need not be used to judge the relative dropout performance of different tapes. In addition to the use of dropout length for simultaneous detection, the length can be used as the criteria for distinguishing between short 4 dB dropouts observed for calendaring impressions and the longer dropouts produced by the circular or elliptical tenting effect caused by small projecting deposit defects, the occasional large diameter depression, and large patches of thin deposits or surface roughness. Similar results can be achieved with the analog approach by incorporating RC networks at the 4 dB inputs to the adder.

6.5 Measurements of Phase Related Bit Errors

High densities of small scale features are present on the subject tapes, such as swales on Fuji H621, and gouges, agglomerates and calendering marks on 3M 5198. These features are not associated with 20 dB dropouts, but frequent subthreshold amplitude reductions have been ascribed to the calendering marks, and changes in reproduction phase are conceivable. Changes in head-to-tape separation caused by surface roughness, anomalous particle orientation, packing factor or dispersion may contribute to phase changes, and those properties may have an even greater effect when combined with peak shift and pulse crowding phenomena associated with HDDR packing densities.

A single inaccurately reproduced bit resulting from the tape anomalies should be detectable and correctable with suitable HDDR codes, but the high density of swales, gouges and agglomerates, and the large size of calendering marks, suggests a statistical possibility of several inaccurate bits within a single code block such that the errors cannot be corrected or are transparent to the error detection code.

The high density of small surface features, the approximations employed in analytical models of the record/reproduce process, and the low precision typical of microanalytical methods may prevent the association of a given reproduced phase error with a particular feature. However, detection and counting of signal phase shifts in the tapes will be implemented. A test series with a standardized phase error detection threshold will provide a comparative measure of the excessive phase shifts induced by anomalies in each tape type. It may also be possible to observe counting patterns and attribute phase shifts to a particular source. For example, with a 60 ips tape speed, repeating calendering defects on 3M 5198 may produce integer multiples of 1.4 or 1.6 events per second at regular intervals. If phase shifts do not occur in a recognizable pattern, additional tests with reduced detection thresholds will cause increased phase error counts, and changes in counts may be compared to densities and size distributions of observable anomalies. These comparisons can be combined with considerations or calculations based on analytical models and microanalytical measurements to determine the source of the phase errors.

The detection circuit will require recording the continuous pattern 110110... in the delayed modulation mark (DM-M) code, also known as the Miller Code. At the 33 Kbp/s density simulated during dropout testing, the repeating code sequence is equivalent to 0.5 μ s wide pulses of either polarity with 1.5 μ s periods at a 60 ips tape speed, and this timing will be employed for a rectangular record current of the same amplitude employed for dropout testing. The recorded code includes transition zone pairs separated by one 30 microinch bit length which should be most sensitive to peak shift and pulse crowding phenomena, and to the effects of tape anomalies. These close transition zone pairs will be separated by two bit length intervals which will insure detection of leading or lagging phase shifts as great as one bit length. The detection circuit will consider only leading or trailing edges of the pulse at a given time, but both edges can be considered by a pair of test runs with opposite signal polarity.

The reproduced waveform will be restored to a rectangular single ended signal by the direct reproduce channel of the Honeywell Model 96 recorder followed by a zero crossing detector. Two timing chains will be triggered by alternate pulses, and the chains will end with adjustable width windows centered over the expected time of the next leading edge. Each window will inhibit detection of the edge from the pulse immediately following the pulse that initiated the timing chain ending in that window, and all edges falling outside of the window will be counted as phase errors. For standardized tests, a total window width of one-half bit length is under consideration.